Sustainable Food Technology

ROYAL SOCIETY OF CHEMISTRY

PAPER

View Article Online
View Journal | View Issue

Cite this: *Sustainable Food Technol.*, 2025, **3**, 1416

Xenovolatilomic profiling of Hass avocado (*Persea americana* Mill.) tissues exposed to endosulfan: identification of potential toxicity biomarkers†

Juan Pablo Betancourt Arango, Alejandro Patiño Ospina, Jhon Alexander Fiscal Ladino and Gonzalo Taborda Ocampo *

Introduction: Omics sciences, particularly metabolomics and its subfield volatilomics, investigate small molecules to understand biochemical dynamics. Volatilomics targets volatile organic compounds (VOCs), which act as biomarkers for physiological changes, environmental stress, and xenobiotic exposure. Advances in GC-MS and HS-SPME have enabled precise VOC profiling. A critical issue in food safety is pesticide contamination, notably organochlorines like endosulfan, which bioaccumulate and disrupt plant metabolomes. Hass avocado (*Persea americana* Mill.), rich in lipids and terpenoids, offers an ideal matrix for studying xenovolatilomic responses. *Objective*: This study evaluated volatilomic alterations induced by endosulfan in Hass avocado using headspace solid-phase microextraction (HS-SPME) coupled with gas chromatography-mass spectrometry (GC-MS). It aimed to identify potential toxicity biomarkers associated with pesticide exposure, contributing to rapid, reliable detection methodologies for agricultural products. *Methodology*: Avocado peel, pulp, and seed were experimentally exposed to endosulfan for 8 and 20 days under controlled conditions. VOCs were extracted by HS-SPME and analyzed by GC-MS. Data were processed and subjected to multivariate statistical analyses, including Principal Component Analysis (PCA), Partial Least Squares-Discriminant Analysis (PLS-DA), random forest, variable importance in projection (VIP) scores, and receiver operating characteristic (ROC) curve analysis to identify VOCs differentially expressed under pesticide exposure. *Results*: Random forest and PLS-DA analyses identified five key VOCs as potential toxicity biomarkers: (*E*)-2-octenal (V93), oct-3-en-2-one (V86), decanal (V129), hexanal (V29), and nonanal (V102). These compounds exhibited significant concentration changes based on exposure time (8 and 20 days) and tissue type. Additionally, an unknown compound (VX83) emerged as a potential biomarker requiring future characterization. *Conclusions*: This study constitutes the first xenovolatilomic investigation in Hass avocado and validates the use of (*E*)-2-octenal, oct-3-en-2-one, decanal, hexanal, and nonanal as potential toxicity biomarkers for the early detection of pesticide-induced biochemical alterations. The integration of volatilomic profiling with multivariate statistical and biochemical analyses provides a solid foundation for developing rapid diagnostic tools and advancing computational metabolomics models for predicting pesticide-induced enzymatic inhibition processes. These findings have implications for food safety, export quality assurance, and the economic sustainability of agricultural production systems in regions like Caldas, Colombia.

Received 25th April 2025
Accepted 6th July 2025

DOI: 10.1039/d5fb00163c

rsc.li/susfoodtech

Sustainability spotlight

The increasing presence of pesticide residues in tropical crops like Hass avocado poses a significant threat to food safety, consumer health, and export sustainability. This work presents a novel xenovolatilomic strategy for the early detection of agrochemical contamination by identifying potential toxicity biomarkers through VOC profiling and multivariate analysis. By enabling rapid, non-destructive monitoring of biochemical alterations in food matrices, this study advances sustainable food quality control. It aligns with the UN Sustainable Development Goals (SDGs), particularly Goal 2 (Zero Hunger), Goal 3 (Good Health and Well-being), and Goal 12 (Responsible Consumption and Production), by promoting safe agricultural practices and reducing toxic exposure in food systems. This approach supports long-term food security and environmentally conscious production.

Department of Chemistry, Research Group on Chromatography and Related Techniques, University of Caldas, Manizales, Caldas, Colombia. E-mail: gtaborda@ucaldas.edu.co

† Electronic supplementary information (ESI) available. See DOI: https://doi.org/10.1039/d5fb00163c

1 Introduction

Omics sciences encompass various disciplines that comprehensively analyze the biochemical environment of biological systems, including genomics, transcriptomics, proteomics, and metabolomics.[1] Among these, metabolomics focuses on the exhaustive study of small molecules known as metabolites, which play key biochemical roles and reflect dynamic changes in cellular physiology.[2] Advances in this field have led to the emergence of specialized subfields such as lipidomics (lipid analysis), peptidomics (peptide profiling), and volatilomics (characterization of volatile organic compounds, VOCs).[3]

Volatilomics has gained relevance in diverse areas, including ecological interactions, environmental quality assessment, natural product bioprospecting, and food safety. This discipline is based on analyzing VOCs, which are naturally emitted by organisms and biological matrices, and whose presence and concentration can indicate physiological alterations.[3] It enables the evaluation of differential metabolite expression in response to environmental factors, physiological stress, and contaminant exposure.[4] In this context, VOCs have also been employed as tools in taxonomic and ecological studies across different species.[5] More recently, specialized volatilomic approaches have emerged, such as exhalomics (analysis of VOCs in exhaled air) and xenovolatilomics, which examines volatile profiles induced by xenobiotic agents.[6] These approaches have been integrated with multi-omics strategies, combining volatilomics with lipidomics and other disciplines to gain a deeper understanding of chemical variability in biological and food samples.[7]

The characterization of VOCs requires advanced extraction and analytical methodologies. Among them, solid-phase microextraction in static headspace (SHS-SPME) and dynamic headspace (DHS-SPME) are widely used for VOC collection due to their sensitivity, reproducibility, and solvent-free operation. For compound identification, gas chromatography (GC) remains the primary technique, often coupled with various detection systems such as mass spectrometry (MS),[8] time-of-flight mass spectrometry (TOF/MS), triple quadrupole mass spectrometry (QTOF/MS),[9] Orbitrap-MS, tandem mass spectrometry (MS/MS), and ion mobility spectrometry (MS-IMS).[10] These platforms enable comprehensive structural elucidation of VOCs and in-depth exploration of the chemical behavior of biological samples. In terms of quantification, gas chromatography with flame ionization detection (GC-FID),[11] is widely regarded as a robust technique due to its excellent linearity and reproducibility across a wide concentration range. Additionally, GC-MS operated in selected ion monitoring (SIM),[12] mode enhances quantification by providing improved sensitivity and selectivity for targeted analytes. The combination of GC-FID and GC-MS (in SIM mode) is often employed to leverage the strengths of both techniques—GC-MS for compound identification and GC-FID or targeted MS modes for accurate quantification—thereby ensuring reliable and reproducible data. Volatilomic analysis is further supported by advanced statistical tools, including both supervised and unsupervised methods. Techniques such as principal component analysis (PCA), hierarchical cluster analysis (HCA), and linear discriminant analysis (LDA) allow for pattern recognition, sample classification, and evaluation of the variables contributing to chemical differentiation between groups.[13]

One of the major challenges in food safety today is the presence of pesticide residues in agricultural crops. Organophosphate and organochlorine pesticides have been extensively used for pest control, yet their uncontrolled application raises concern due to their accumulation in fruits, vegetables, and other agricultural products.[14] These compounds, being foreign to biological systems, are classified as xenobiotics and can induce biochemical alterations in exposed organisms, even at low concentrations.[15] Globally, organochlorine pesticides such as endosulfan have been restricted or banned in many countries due to their high persistence, lipophilicity, and tendency to bioaccumulate within ecosystems and food chains.[16] The inclusion of endosulfan in the Stockholm Convention on Persistent Organic Pollutants (2011) marked a turning point in international recognition of its environmental and health risks.[17] Nonetheless, residues of endosulfan and its isomers (α, β, and sulfate) continue to be reported in soil, water, and food commodities, particularly in tropical and developing regions. Toxicological studies have demonstrated endosulfan's potential to induce neurotoxicity, reproductive dysfunction, oxidative stress, and enzymatic inhibition in a range of biological systems, including plants, animals, and humans.[18]

In Colombia, pesticide use is regulated to ensure food safety and facilitate international trade in agricultural products. However, organochlorine pesticides such as endosulfan have raised significant environmental and health concerns due to their persistence and bioaccumulation. Notably, endosulfan isomers (α, β, and sulfate) exhibit substantial toxicity to both organisms and ecosystems.[19,20] This situation underscores the need for rapid, cost-effective, and reliable research methods. Xenometabolomic,[21–23] and xenovolatilomic studies provide valuable strategies for identifying secondary metabolites expressed in response to xenobiotic exposure, aiming to develop omics-based methodologies that characterize metabolites for potential toxicity biomarker identification.

Hass avocado (*Persea americana* Mill.) is among the most widely cultivated and commercially significant avocado varieties worldwide, representing a key agro-industrial product in countries such as Colombia, Mexico, and Peru. Its chemical composition, rich in lipids, phenolic compounds, and terpenoids, makes it an ideal model for volatilomic studies, as its VOCs are associated with quality, ripening, and environmental responses. However, avocado production is exposed to pesticide applications for pest and disease control, raising concerns about potential pesticide residues in the fruit.[24] Notably, endosulfan has been identified as an environmental contaminant in avocado crops, with the potential to alter its metabolism and volatilomic profile. Xenovolatilomic studies have demonstrated that pesticide exposure can induce the formation of specific VOCs, which may serve as biomarkers of contamination and toxicity. In this regard, Hass avocado serves as an optimal matrix for evaluating volatilomic profile alterations induced by

endosulfan, with the aim of identifying potential toxicity biomarkers.

A toxicity biomarker,[25] is characterized as a response metabolite that emerges in the presence of a xenobiotic agent. These biomarkers provide a rapid methodology for early detection of contamination in samples exposed to xenobiotic agents such as pesticides. This study conducted a xenovolatilomic analysis of Hass avocado (*Persea americana* Mill.) using headspace solid-phase microextraction (HS-SPME) and gas chromatography-mass spectrometry (GC-MS).[26] The objective is to assess alterations in the volatilomic profile induced by endosulfan and its potential for identifying toxicity biomarkers in this fruit.

2 Methodology

2.1 Sampling

The *Persea americana* Mill. (Hass variety) samples were sourced from various local markets and distribution centers in Manizales, Caldas, Colombia. Additional fruit samples were provided by the Department of Agriculture of Caldas from the municipalities of Pácora, Aranzazu, and Salamina. Sampling was conducted between April and May 2024, coinciding with the harvest season. Selection criteria focused on size uniformity and the absence of physical damage or visible disease symptoms. Fruits were transported in sealed containers at approximately 5 °C to minimize metabolic activity and delay respiration. Upon arrival at the laboratory, samples were stored under controlled ambient conditions. To ensure uniform ripening, all fruits were processed at an intermediate ripening stage (level three), characterized by a dark-colored and soft exocarp (peel), a mesocarp (pulp) that remained soft yet firm to the touch, and a fully formed endocarp and seed, both visually free of defects or anomalies. This sampling protocol ensured traceability and standardized ripening, reducing variability associated with uncontrolled physiological changes. A completely randomized design was used for sample selection. The fruits were separated into three anatomical parts: exocarp (peel), mesocarp (pulp), and seed. For each experimental condition (tissue type and exposure time), three independent biological replicates were prepared. Each biological replicate was analyzed in technical triplicate using headspace solid-phase microextraction (HS-SPME) coupled with gas chromatography–mass spectrometry (GC-MS), resulting in nine analytical data points per tissue and exposure period. Quality control (QC) samples were included throughout the analytical sequence to assess reproducibility, detect potential instrumental drift, and ensure overall stability of the method.

2.2 Application of xenobiotic agent

To evaluate the response metabolites (RMs) involved in the development of potential toxicity biomarkers in Hass avocado, controlled exposure experiments were performed. For each tissue type (peel, pulp, and seed), 2.5 g of sample were prepared and treated with 100 μL of endosulfan at a concentration of 1000 mg kg^{-1}. The xenobiotic was allowed to interact with the matrix under controlled laboratory conditions for two exposure periods: 8 and 20 days, respectively. The induction process was carried out under controlled ambient conditions at 25 ± 1 °C and in the absence of light, to prevent temperature- or light-induced degradation or volatilization of the xenobiotic compound. As a control, non-doped Hass avocado samples (not exposed to endosulfan) were included for each tissue type and analyzed in parallel under identical conditions. These control samples served as a baseline to compare against the xenobiotically altered samples, enabling the identification of differentially expressed VOCs. For each treatment condition and tissue type, three independent biological replicates were processed. Each biological replicate was analyzed in technical triplicate using headspace solid-phase microextraction (HS-SPME) coupled with gas chromatography-mass spectrometry (GC-MS), resulting in a total of 9 analytical measurements per matrix and exposure period. In total, 27 doped samples were analyzed across all conditions. Following exposure, the volatile organic compounds (VOCs) were extracted and analyzed, and the resulting data were subjected to multivariate statistical analysis for biomarker identification.

2.3 Extraction of volatile organic compounds (VOCs)

VOCs were extracted using headspace solid-phase microextraction (HS-SPME) with a gray fiber composed of polydimethylsiloxane, divinylbenzene, and carboxen (PDMS/DVB/CARB). For the extraction process, 2.5 g of Hass avocado peel, pulp, and seed were utilized, with 0.4 g of NaCl added to enhance the salting-out effect, followed by homogenization of the mixture. Before extraction, the samples underwent ultrasonic treatment for 20 minutes. The extraction was conducted at 52 °C for 40 minutes, after which the compounds were analyzed by GC-MS. Desorption was performed at 250 °C for 15 minutes in the instrument's injection port. To ensure the reproducibility of VOC extraction, separation, and identification, this procedure was performed in triplicate for each sample, including both commercially available avocados and those sourced from the northern subregion of Caldas.

2.4 Gas chromatography-mass spectrometry GC-MS analysis

The separation and detection of VOCs in Hass avocado were carried out using a Shimadzu Thermo Scientific™ TRACE™ QP2010 Plus gas chromatograph (GC) coupled with a mass spectrometry (MS) detector. The analysis was conducted with a ZB-5 capillary column (30 m × 0.25 mm ID × 0.25 μm film thickness). A temperature gradient program was implemented to optimize compound separation. The initial oven temperature was set at 45 °C for 2 minutes, followed by an increase of 3 °C min^{-1} until reaching 100 °C, where it was maintained for 1 minute. Subsequently, the temperature was raised to 300 °C at a rate of 10 °C min^{-1} and held for 2 minutes, resulting in a total runtime of 43.33 minutes. The injection was performed in solid-phase microextraction (SPME) mode, utilizing helium as the carrier gas. The injection port was maintained at 250 °C, while the mass spectrometer detector operated at 290 °C. Compound detection was performed in scan mode using electron impact ionization (EI) at 70 eV.

2.5 Identification of toxicity biomarkers

The identification of VOCs obtained through HS-SPME-GC-MS was conducted using Solution Version 4.30 software from the Shimadzu Thermo Scientific™ TRACE™ QP2010 Plus system. Compound identification was performed by referencing the NIST14 library, applying an 80% similarity threshold, as well as the NIST14S, ADAMS, ESSENTIAL OILS, and FFNSC (Flavour and Fragrance Natural and Synthetic Compounds) libraries, where a stricter 90% similarity threshold was used. Peak smoothing and area integration were executed using the software. Additionally, a series of alkanes was analyzed to determine Kovats retention indices (KI). To enhance compound identification validation, the data were further processed through the Global Natural Products Social Molecular Networking (GNPS) database.[27] This approach enabled peak deconvolution, identification of GC-MS data, and the construction of a molecular network to correlate the VOCs present in the peel, pulp, and seed of Hass avocado. For the final compound report, the following parameters were documented: compound name, molecular formula, mass-to-charge ratio (*m/z*), boiling point (BP), retention time (RT), theoretical Kovats index (Theo KI), experimental Kovats index (Exp KI), similarity percentage (SI), peak area, adduct type, reference to Human Metabolome Database (HMDB), and percentage of error on the kovats index.

2.6 Quality assurance and quality control

To ensure the accuracy and reliability of the results obtained in this study, a rigorous quality assurance (QA) and quality control (QC) protocol was established. This protocol involved the use of quality control samples, instrument performance verification, and data validation procedures. A total of 35 quality control samples were analyzed. For gas chromatography (GC) analysis, quality control measures were distributed as follows: 10 column quality controls (CQC) and 12 system quality controls (SQC) to assess instrument response through solvent injections. Given that VOC extraction was conducted *via* HS-SPME, an additional 13 fiber quality controls (FQC) were implemented to verify injection integrity and prevent potential carryover effects caused by compound retention on the fiber surface between samples. These quality control measures facilitated the assessment of chromatographic system stability and the detection of background contamination within the column. CQC samples consisted of blank injections to monitor column performance and identify any potential cross-contamination between samples. SQC samples contained only the solvent (acetone) used for column cleaning and were injected to detect and correct background noise, eliminate contaminants between volatilomic sample injections, and evaluate signal variation in the analytical instrument.

2.7 Structural analysis of metabolites

The identified metabolites were assigned their respective HMDB and KEGG (Kyoto Encyclopedia of Genes and Genomes) codes (**https://www.genome.jp/kegg/**).[28] This information was uploaded to the MetaboAnalyst 6.0 platform (**https://www.metaboanalyst.ca/**),[29] enabling an enrichment analysis of the metabolite set to identify the major chemical families present within the xenovolatilomic profiles and to assess the statistical significance of each family. Additionally, a bubble plot was generated to visualize the statistical significance of metabolite classes and the relative enrichment size in relation to the total number of metabolites analyzed.

2.8 Multivariate analysis

Data processing was conducted using the Python programming language through the development of custom scripts. These scripts enabled data importation, information verification, removal of missing values, scaling, normalization, and assessment of multivariate normality. Subsequently, exploratory non-parametric multivariate techniques such as Principal Component Analysis (PCA) and a scree plot were applied to evaluate the contribution of each variable to the principal components. Additionally, non-parametric analyses were performed using Hierarchical Cluster Analysis (HCA) and random forest, along with parametric analysis *via* Partial Least Squares Discriminant Analysis (PLS-DA). Following the application of these techniques, Variable Importance in Projection (VIP) scores were calculated from both the PLS-DA and random forest models to identify the importance of independent variables in explaining the dependent variable across the model components. Finally, after constructing the models and ensuring a balanced distribution of treatment classes (doped and undoped samples), cross-validation was performed to evaluate the predictive capacity of the models on this dataset.

2.9 Potential toxicity biomarkers

Based on the identification of VIP scores obtained from the PLS-DA and random forest models, the main compounds contributing to the variability and classification of samples categorized as doped and undoped were established. Subsequently, statistical verification and validation of the identified potential toxicity biomarkers were performed by applying the non-parametric Mann–Whitney test to determine significant differences between the two independent groups. Additionally, Receiver Operating Characteristic (ROC) curve analysis was conducted to assess the performance of each biomarker as a binary classifier, complemented by the calculation of the Area Under the ROC Curve (AUC-ROC) to quantify the overall discriminative power of each potential biomarker.

2.10 Metabolic pathway analysis

The KEGG, HMDB, Lipid Maps, and MetaCyc codes for each identified metabolite were obtained using the Chemical Entities of Biological Interest (ChEBI) database (**https://www.ebi.ac.uk/chebi/**). To perform a xenovolatilomic analysis and identify the different metabolic alterations induced in the biochemical pathways of the peel, pulp, and seed of Hass avocado, a Python-based script was developed to search for metabolite codes within the KEGG, HMDB, Lipid Maps, and MetaCyc databases. Subsequently, the script extracted metabolite

Table 1 Metabolites identified in the peel, pulp, and seed of Hass avocado after eight days of exposure to endosulfan

	Peel with endosulfan 8 days				Pulp with endosulfan 8 days				Seed with endosulfan 8 days			
Compound number	Name	Code KEGG/Lipid Maps/ HMDB/MetaCyc	RT	KI	Name	Code KEGG/Lipid Maps/ HMDB/MetaCyc	RT	KI	Name	Code KEGG/Lipid Maps/ HMDB/MetaCyc	RT	KI
1	(2*E*)-Hexenal	HMDB0031496	7.118	847	2,2-Dimethylhexane	—	3.205	705.8	2,2,4-Trimethylpentane	—	3.224	706.5
2	(2*E*)-Heptenal	LMFA06000019	11.261	959	Hexanal	LMFA06000109	5.424	791.6	Hexanal	LMFA06000109	5.424	791.6
3	Benzaldehyde	C00261	11.580	967	(2*E*)-Hexenal	HMDB0031496	7.118	847.1	(2*E*)-Hexenal	HMDB0031496	7.118	847.1
4	Beta-myrcene	C06074	12.590	991	(2*E*)-Heptenal	LMFA06000019	11.261	959.3	Alpha-pinene	C09880	9.996	929.1
5	Eucalyptol	C09844	14.525	1033	Benzaldehyde	C00261	11.580	966.9	(2*E*)-Heptenal	LMFA06000019	11.261	959.3
6	(*Z*)-Beta-ocimene	—	14.875	1041	1-Octen-3-ol	LMFA05000090	12.595	991.2	Benzaldehyde	C00261	11.580	966.9
7	(*E*)-Beta-ocimene	LMPR0102010021	15.285	1050	Oct-3-en-2-one	HMDB0033547	14.940	1042	(−)-Beta-pinene	C06307	12.015	977.3
8	(*E*)-2-Octenal	HMDB0013809	15.995	1065	(*E*)-2-Octenal	HMDB0013809	15.995	1065	Beta-myrcene	C06074	12.590	991.1
9	Nonanal	LMFA06000040	18.140	1111	Nonanal	LMFA06000040	18.140	1111	1,4,4-Trimethyl-3,5-dimethylenecyclopentene	—	14.160	1026
10	Decanal	HMDB0011623	22.870	1216	1-Chlorodecane	—	20.875	1168	Limonene	HMDB0004321	14.505	1033
11	Alpha-ylangene	HMDB0301856	26.940	1379					(*Z*)-Beta-ocimene	—	14.875	1041
12	(−)-Alpha-copaene	HMDB0061851	27.060	1385					Oct-3-en-2-one	HMDB0033547	14.940	1042
13	1,5-Di-*epi*-bourbonene	—	27.215	1393					(*E*)-2-Octenal	HMDB0013809	15.995	1065
14	(−)-Beta-elemene	HMDB0061848	27.305	1397					4-Methyl-3-(1-methylethylidene)-1-cyclohexene	—	17.020	1087
15	(−)-*trans*-Caryophyllene	C09629	27.875	1432					Dehydro-*p*-cymene	HMDB0029641	17.325	1093
16	(+)-Delta-cadinene	C06394	29.413	1533					Nonanal	LMFA06000040	18.140	1111
17	Zonarene	HMDB0303004	29.465	1537					4,8-Dimethyl-1,3,7-nonatriene	—	18.500	1118
18	Methyl palmitate	HMDB0061859	34.175	1937					Alpha-pinocarvone	C09884	20.830	1167
19	Tetratriacontane	LMFA11000587	40.935	2712					*n*-Decanal	HMDB0011623	22.870	1216
20									Octyl acetate	LMFA07010197	22.985	1220
21									1,9-Decadiene	HMDB0244254	25.095	1291
22									10-Undecenal	HMDB0031128	25.598	1312
23									Alpha-ylangene	HMDB0301856	26.940	1379
24									(−)-Alpha-copaene	HMDB0061851	27.060	1385
25									Beta-maaliene	—	27.233	1394
26									Decyl acetate	LMFA07010212	27.640	1418
27									Opposita-4(15),7-diene	—	27.900	1434
28									Selina-4(15),7-diene	—	28.512	1472
29									Alpha-amorphene	CPD-8797	28.735	1486
30									(+)-Delta-cadinene	C06394	29.413	1533
31									(*Z*,*Z*)-1,8,11-Heptadecatriene	HMDB0302479	31.220	1672
32									*cis*-11-Tetradecen-1-ol	—	31.475	1692

Table 2 Metabolites identified in the peel, pulp, and seed of Hass avocado after twenty days of exposure to endosulfan

	Peel with endosulfan 20 days				Pulp with endosulfan 20 days				Seed with endosulfan 20 days			
Compound number	Name	Code KEGG/Lipid Maps/ HMDB/MetaCyc	RT	KI	Name	Code KEGG/Lipid Maps/ HMDB/MetaCyc	RT	KI	Name	Code KEGG/Lipid Maps/ HMDB/MetaCyc	RT	KI
1	2,2-Dimethylhexane	—	3.205	706	2,2-Dimethylhexane	—	3.205	705.8	Pentanal	HMDB0031206	3.400	713.3
2	Pentanal	HMDB0031206	3.400	713	Pentanal	HMDB0031206	3.400	713.3	Pentanol	—	4.935	772.7
3	*trans*-2-Pentenal	CPD-13228	4.393	752	Pentanol	—	4.930	772.5	Hexanal	LMFA06000109	5.424	791.6
4	Pentanol	—	4.935	773	Hexanal	LMFA06000109	5.424	791.6	Furfural	C14279	6.850	838.6
5	Hexanal	LMFA06000109	5.424	792	Furfural	C14279	6.850	838.6	(2*E*)-Hexenal	HMDB0031496	7.118	847.1
6	(2*E*)-Hexenal	HMDB0031496	7.118	847	(2*E*)-Hexenal	HMDB0031496	7.118	847.1	2-Heptanone	LMFA12000004	8.340	886.1
7	2-Heptanone	LMFA12000004	8.340	886	Heptanal	HMDB0031475	8.885	902.6	Heptanal	HMDB0031475	8.885	902.6
8	Heptanal	HMDB0031475	8.885	903	Cyclohexane carboxaldehyde	—	10.500	941.2	Pentyl acetate	—	9.290	912.3
9	(*E*)-2-Heptenal	LMFA06000019	11.261	959	(*E*)-2-Heptenal	LMFA06000019	11.261	959.3	Alpha-pinene	C09880	9.988	928.9
10	Benzaldehyde	C00261	11.580	967	Benzaldehyde	C00261	11.580	966.9	Cyclohexane carboxaldehyde	—	10.500	941.2
11	1-Octen-3-ol	LMFA05000090	12.595	991	Octanal	HMDB0001140	13.785	1018	(*E*)-2-Heptenal	LMFA06000019	11.261	959.3
12	Octanal	HMDB0001140	13.785	1018	5-Ethyl-1-formylcyclopentene	—	14.520	1033	Benzaldehyde	C00261	11.580	966.9
13	(2*E*,4*E*)-Hepta-2,4-dienal	LMFA06000024	13.771	1017	Oct-3-en-2-one	HMDB0033547	14.940	1042	(−)-Beta-pinene	LMPR0102120013	12.015	977.3
14	Oct-3-en-2-one	HMDB0033547	14.940	1042	(*E*)-2-Octenal	HMDB0013809	15.995	1065	Oct-1-en-3-one	HMDB0031309	12.065	978.5
15	(*E*)-2-Octenal	HMDB0013809	15.995	1065	Nonanal	LMFA06000040	18.140	1111	Octanal	HMDB0001140	13.785	1018
16	Nonanal	LMFA06000040	18.140	1111	(*Z*)-Non-2-enal	LMFA06000041	20.840	1167	*o*-Cymene	HMDB0037050	14.160	1026
17	(*E*)-2-Nonenal	LMFA06000041	20.910	1169	Decanal	HMDB0011623	22.870	1216	5-Ethyl-1-formylcyclopentene	—	14.520	1033
18	Decanal	HMDB0011623	22.870	1216	(*E*)-2-Decenal	LMFA06000053	24.650	1276	Oct-3-en-2-one	HMDB0033547	14.940	1042
19	Octyl acetate	LMFA07010197	22.985	1220	Undecan-6-one	LMFA12000062	24.805	1281	Benzeneacetaldehyde	C00601	15.262	1049
20	(*E*)-Dec-2-enal	LMFA06000053	24.650	1276					(*E*)-2-Octenal	HMDB0013809	15.995	1065
21	(+)-Cyclosativene	HMDB0302487	26.935	1379					Dehydro-*p*-cymene	HMDB0029641	17.325	1093
22	(−)-Alpha-copaene	HMDB0061851	27.060	1385					(*Z*)-4-Decenal	HMDB0041014	22.415	1201
23	(−)-*trans*-Caryophyllene	C09629	27.875	1432					Decanal	HMDB0011623	22.870	1216
24	*trans*-Alpha-bergamotene	—	28.050	1443					Acetic acid octyl ester	LMFA07010197	23.000	1221
25	(+)-Delta-cadinene	C06394	29.413	1533					(*E*)-Dec-2-enal	LMFA06000053	24.650	1276

Table 2 (*Contd.*)

Compound number	Peel with endosulfan 20 days				Pulp with endosulfan 20 days				Seed with endosulfan 20 days			
	Name	Code KEGG/Lipid Maps/ HMDB/MetaCyc	RT	KI	Name	Code KEGG/Lipid Maps/ HMDB/MetaCyc	RT	KI	Name	Code KEGG/Lipid Maps/ HMDB/MetaCyc	RT	KI
26	Zonarene	HMDB0303004	29.465	1537					10-Undecenal	HMDB0031128	25.598	1312
27	Phytone	—	33.305	1855					(−)-Alpha-copaene	HMDB0061851	27.060	1385
28									(*Z*)-Dec-4-enyl ethyl carbonate	—	27.265	1395
29									*trans*-Alpha-bergamotene	—	28.050	1443
30									Selina-4(15),7-diene	—	28.580	1476
31									(+)-Alpha-muurolene	CPD-8798	28.795	1490
32									(+)-Delta-cadinene	C06394	29.413	1533
33									1-Heptadecanol	—	33.765	1897
34									Eicosane	HMDB0059909	33.875	1908
35									Tetratriacontane	LMFA11000587	40.935	2712

information, identifying the biosynthetic pathways and the enzymes involved in each process. This approach enabled the localization of the potential toxicity biomarkers identified in this study within their corresponding biochemical pathways and allowed the correlation of these biomarkers with possible metabolic blockages and enzymatic alterations induced by exposure to endosulfan as a xenobiotic contaminant. Additionally, a pathway-targeted analysis was performed using the MetaboAnalyst 6.0 platform, integrating enrichment and pathway topology analyses to visualize the general metabolic pathways represented by the identified metabolites within both xenovolatilomic profiles evaluated.

3 Results and discussion

3.1 Metabolites comprising the xenovolatilome

The GC-MS signals were processed using the previously mentioned libraries, with a similarity index threshold of 90%, determining the mass-to-charge ratio (m/z) and retention time for each experimentally detected signal. The identity of each compound was confirmed by comparing both theoretical and experimental fragmentation patterns. Additionally, Kovats Index (KI) values were compared, with the experimental KI calculated by interpolating each signal relative to a series of alkanes (C_7–C_{40}). Compounds were confirmed when their experimental KI values deviated by less than 10% from the theoretical values.

As additional information, for each metabolite identified, key data were collected including the PubChem ID, common name, signal-to-noise ratio (S/N), molecular formula, and the corresponding codes from HMDB, KEGG, Lipid Maps, and MetaCyc, in order to support the construction of associated biochemical pathways. Details regarding both identified and unidentified xenovolatilomic metabolites observed during the two exposure periods are provided in the ESI.†

Specifically, metabolite data for peel (Tables S1 and S2), pulp (Tables S3 and S4), and seed (Tables S5 and S6†) are included to document changes across tissues and exposure times. Tables 1 and 2, summarize the xenovolatilomic profiles of Hass avocado peel, pulp, and seed after 8 and 20 days of endosulfan exposure, respectively. After 8 days, a total of 19 compounds were identified in the peel, 10 in the pulp, and 32 in the seed. After 20 days, the number of compounds increased to 27 in the peel, 19 in the pulp, and 35 in the seed, reflecting a time-dependent metabolic response. This progressive increase in detected VOCs may be attributed to the cumulative oxidative stress induced by prolonged exposure to endosulfan, leading to sustained lipid peroxidation, enzymatic inhibition, and continued formation of aldehydes, ketones, and secondary volatile metabolites. Fig. 2 provides a visual representation of the overlap and distribution of identified VOCs among the three fruit tissues after 8 days (Fig. 2A) and 20 days (Fig. 2B) of exposure, illustrating the interconnectedness and potential metabolic convergence triggered by the xenobiotic agent.

As shown in Fig. 2, increasing the exposure time to the xenobiotic leads to a significant rise in the number of detected metabolites in each fruit section. However, some of these

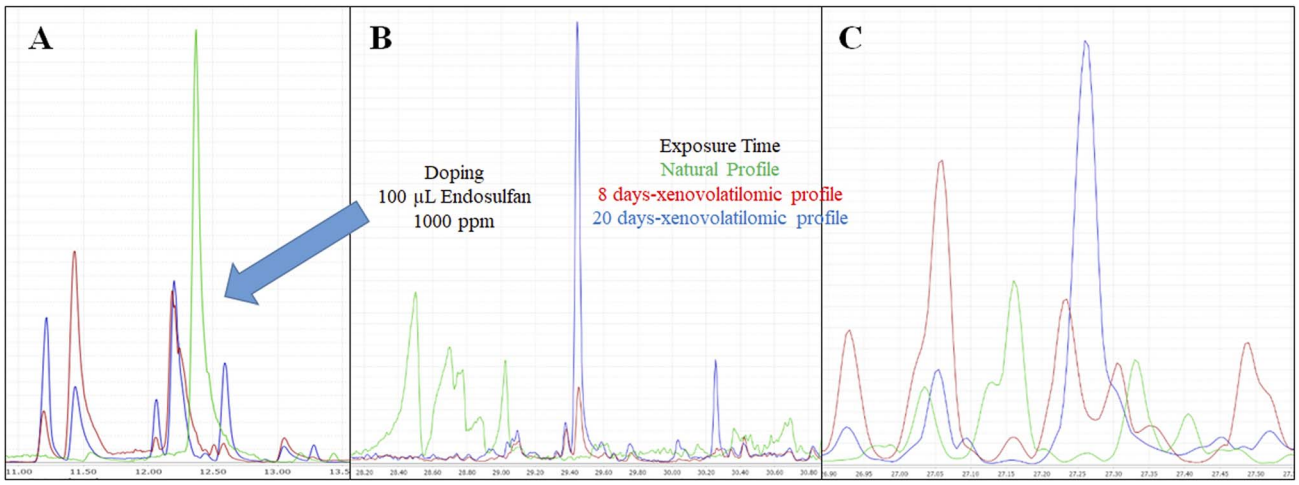

Fig. 1 Comparison of the natural volatilomic profile (green) with the xenovolatilomic profiles after 8 days (red) and 20 days (blue) of exposure to endosulfan, obtained by GC-MS. (A) Peel. (B) Pulp. (C) Seed.

metabolites begin to appear in all three parts simultaneously, indicating the formation of new, biochemically correlated compounds shared across tissues. The variations observed in the volatilomic profiles (Fig. 1) reflect this temporal differentiation, with new signals emerging and others disappearing as exposure time increases. This behavior results from metabolic fluxes in which endosulfan interacts with the natural cellular biochemical pathways in the peel, pulp, and seed of Hass avocado. This interaction triggers the generation of response metabolites (RMs), which act as potential toxicity biomarkers in response to the biological and biochemical alterations induced by the pesticide.

Additionally, in xenovolatilomic profile 1 (Fig. 2A), 9 unique metabolites were identified in the peel, 3 in the pulp, and 20 in the seed, with the seed showing the highest volatile diversity under this condition. Five common metabolites were also found across the three tissues. In xenovolatilomic profile 2 (Fig. 2B), 9 VOCs were unique to the peel, 3 to the pulp, and 16 to the seed. The seed exhibited a reduction in metabolites after 20 days of exposure, suggesting possible metabolization or biotransformation over time. A total of 11 metabolites were common to all three fruit parts, representing a significant increase compared to profile 1. This analysis indicates a notable increase in the number of shared metabolites among the different fruit tissues

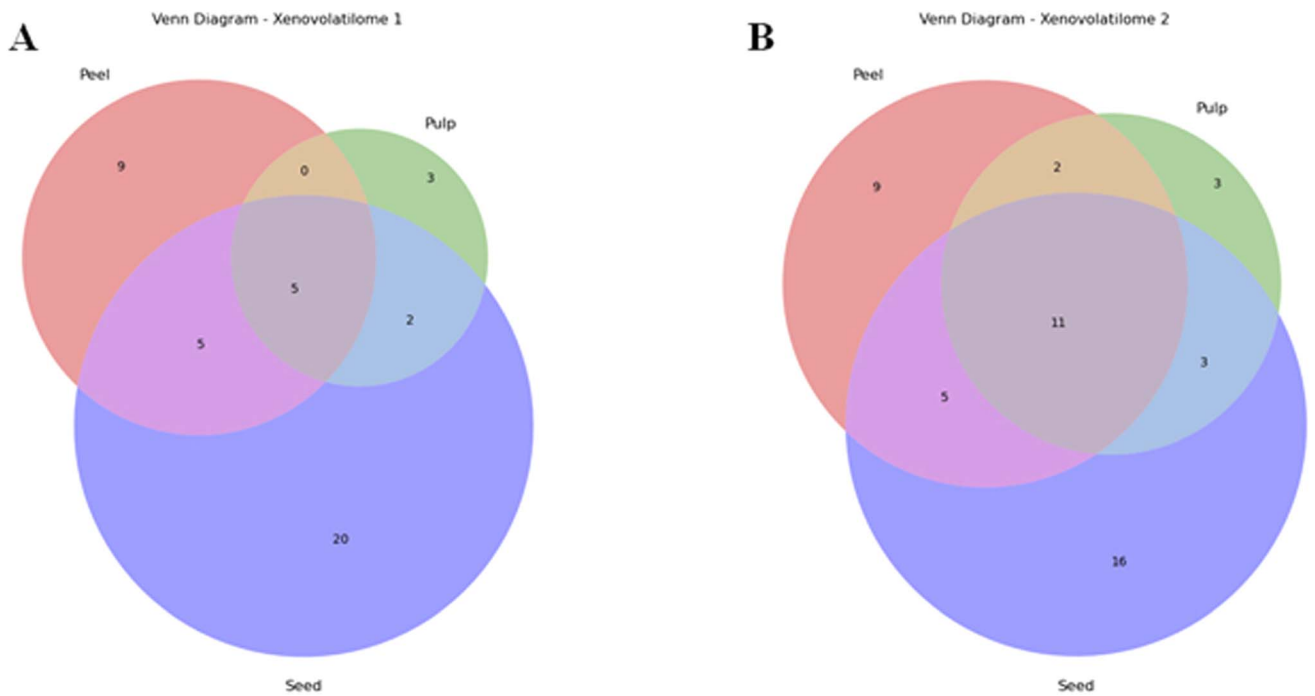

Fig. 2 Venn diagram showing the interconnection of metabolites across the different fruit tissues. (A) Xenovolatilomic profile 1 in Hass avocado after 8 days of exposure to endosulfan. (B) Xenovolatilomic profile 2 in Hass avocado after 20 days of exposure to endosulfan.

as exposure progresses, which could be attributed to the diffusion or migration of compounds, biotransformation processes, or a convergent adaptive response of the fruit matrices to the presence of the xenobiotic.[30–33]

3.2 Structural analysis of xenovolatilome metabolite constituents

Fig. 3A displays a horizontal bar plot illustrating the distribution of different metabolite classes grouped by chemical family. The results indicate that the phenylpropenes family is the most enriched (represented by the longest bar) with a low *p*-value, making it highly significant. Other relevant, though less significant, classes include phenylacetaldehydes, cumenes, and benzoyl derivatives. Fig. 3B shows a bubble plot representing the statistical significance of the identified metabolite classes. In this plot, the size of each bubble represents the enrichment ratio, while the color of the bubble indicates the *p*-value, ranging from yellow (less significant) to red (highly significant). Both the enrichment analysis and the *p*-value calculations were performed using the MetaboAnalyst 6.0 platform, which applies hypergeometric testing and pathway topology algorithms to evaluate statistical significance based on chemical similarity.

The bubble plot results indicate that carbonyl compounds and monoterpenoids exhibit the lowest *p*-values (expressed as $-\log(p)$) and relatively small bubble sizes, suggesting that these compound families are statistically significant, although less enriched. In contrast, phenylpropenes stand out due to their high level of significance and representativeness within the xenovolatilome, whereas fatty acid esters display low significance and minimal enrichment. These results indicate that these volatile compound families are significantly present in the xenovolatilome of Hass avocado during both exposure periods, with a strong dominance of phenylpropenes-type VOCs, followed by other aromatic compounds such as phenylacetaldehydes and cumenes. The enrichment analysis of these compounds suggests a specific chemical response of the fruit to stress induced by the xenobiotic agent, indicating a relationship with metabolic defense mechanisms, lipid oxidation processes, and enzymatic detoxification pathways.

3.3 Multivariate analysis

3.3.1 Principal component analysis (PCA). Multivariate analysis was performed on a dataset comprising 33 samples each of peel, pulp, and seed, along with 10 CQC, 13 FQC, 12 SQC, and 27 doped samples of Hass avocado. This dataset contained volatilomic profiles of natural Hass avocado samples collected from the northern subregion of Caldas, specifically from the municipalities of Pacora, Aranzazu, and Salamina, as well as xenovolatilomic profiles from peel, pulp, and seed exposed to the pesticide endosulfan under two different exposure periods. Data processing was carried out using Python programming language, with a custom script developed to normalize the dataset through *Z*-score standardization, appropriate for multivariate data handling. The multivariate normality of the data was evaluated using the Henze–Zirkler (HZ) test, which yielded a *p*-value < 0.05, indicating that the data did not follow a normal distribution and therefore required the use of non-parametric multivariate statistical methods. Based on this, the data distribution was explored using Principal Component Analysis (PCA) (Fig. 4). The first principal

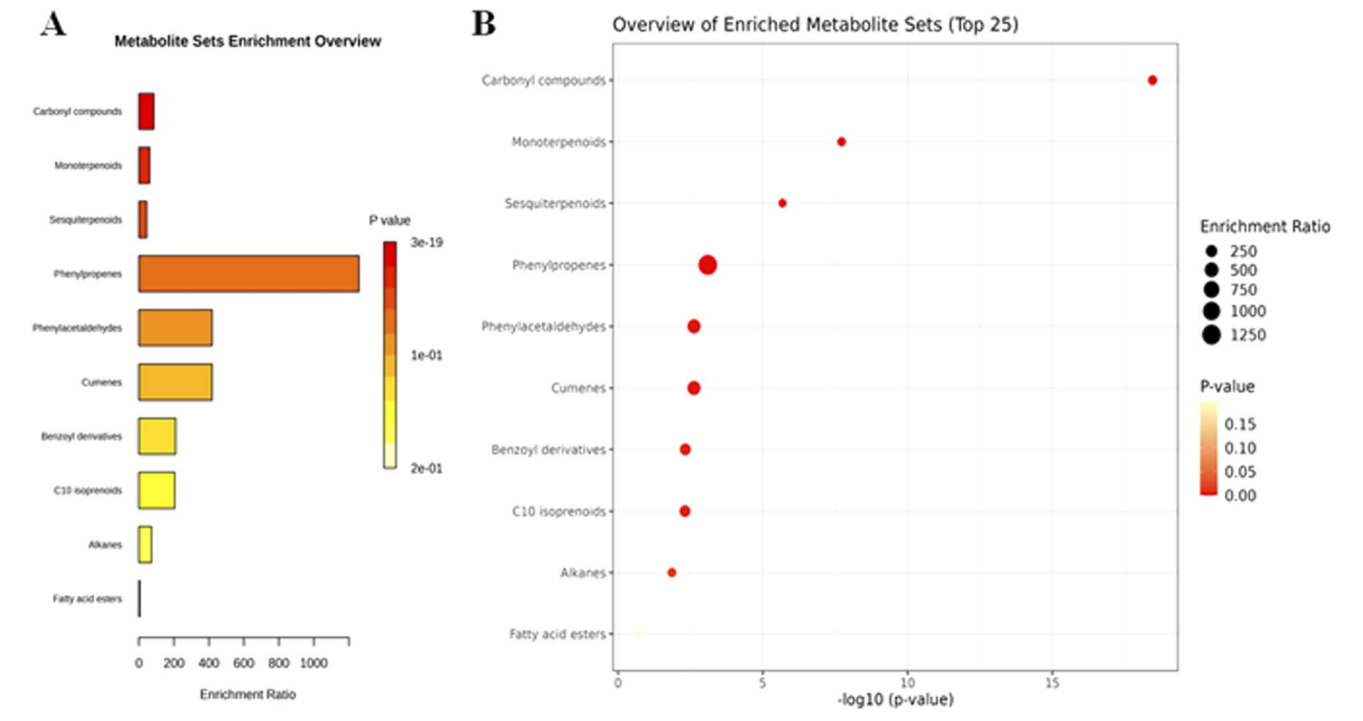

Fig. 3 (A) Summary of the enrichment analysis performed on the metabolite set. (B) Bubble plot showing the significance analysis of the enriched metabolite classes.

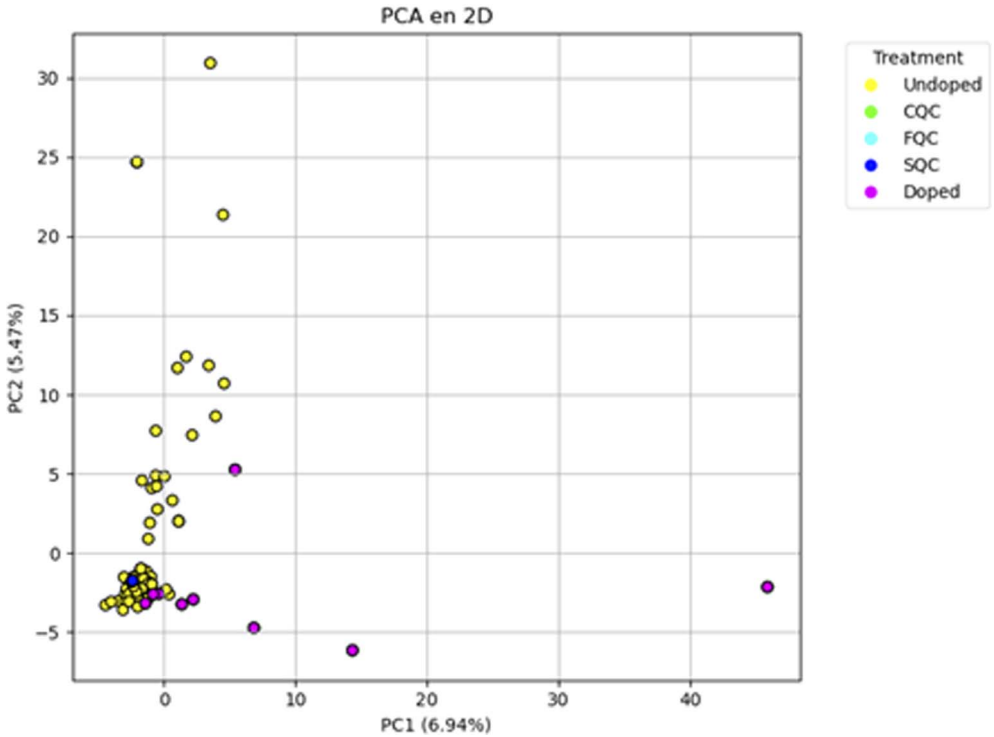

Fig. 4 Principal component analysis (PCA) of the dataset comparing doped and undoped samples.

component (PC1) accounted for 6.94% of the total variance, while the second principal component (PC2) explained 5.47% of the total variance within the set of doped and undoped samples exposed to the xenobiotic agent.

Although the total explained variance is relatively low (12.4%), the analysis allows for a preliminary visualization of distribution patterns and groupings among the samples. The information represented in the PCA is validated by the different quality controls applied (CQC, FQC, and SQC), confirming the absence of instrumental interferences, ensuring high reproducibility of the technique, verifying the quality of the experiments performed, and supporting the validity of the model without noise interference from the technique or the biological samples themselves. Additionally, the PCA shows clear differentiation between doped and undoped samples, indicating that the endosulfan doping applied to the peel, pulp, and seed samples distinctively and consistently affects the volatilomic profile of these plant matrices.

3.3.2 Main contributors to variability. Fig. 5A displays the 60 most representative variables for each component, with PC1 (blue bars) and PC2 (red bars), indicating which variables exert the greatest influence on sample separation along each principal component. Variables were classified based on their identification codes as identified volatile metabolites (V) and unidentified volatile metabolites (VX). Notably, the metabolites V139, V231, V206, V132, V135, V251, and V49, along with the unidentified compounds VX257, VX129, VX185, VX379, VX223, and VX194, contributed most to the variability explained by PC1. For PC2, the metabolites V64, V109, V89, and V215 showed the strongest positive influence on the distribution of the data. The scree plot (Fig. 5B) illustrates the variance explained by each individual principal component, indicating that more than three components are needed to adequately explain the behavior of the biological data analyzed. However, for exploratory purposes, this study focuses on the first two components. Fig. 5C shows the cumulative variance analysis, representing the progressive summation of variance explained by each component. The dashed line marks the 95% cumulative variance threshold, a typical benchmark for retaining sufficient information. This suggests that approximately 50 components would be required to explain the total accumulated variance—a pattern commonly observed in large datasets from metabolomic and volatilomic studies.

3.3.3 Sample differentiation. To explore the differentiation between samples, a hierarchical cluster analysis (HCA) was performed (Fig. 6A), displaying a dendrogram that groups the samples based on their volatilomic similarity. Samples positioned closer together horizontally are more strongly correlated, revealing clustering patterns among the peel, pulp, and seed samples from the subregions of Pácora, Aranzazu, and Salamina. Likewise, a clear separation is observed between doped and undoped samples, indicating that the treatment significantly altered the chemical profile of Hass avocado, allowing differentiation between treated and natural samples while also highlighting the internal similarity within each fruit tissue profile.

To further assess treatment separation, a Partial Least Squares Discriminant Analysis (PLS-DA) was applied (Fig. 6B). This plot projects the samples into a reduced-dimensional space, maximizing differences between predefined groups:

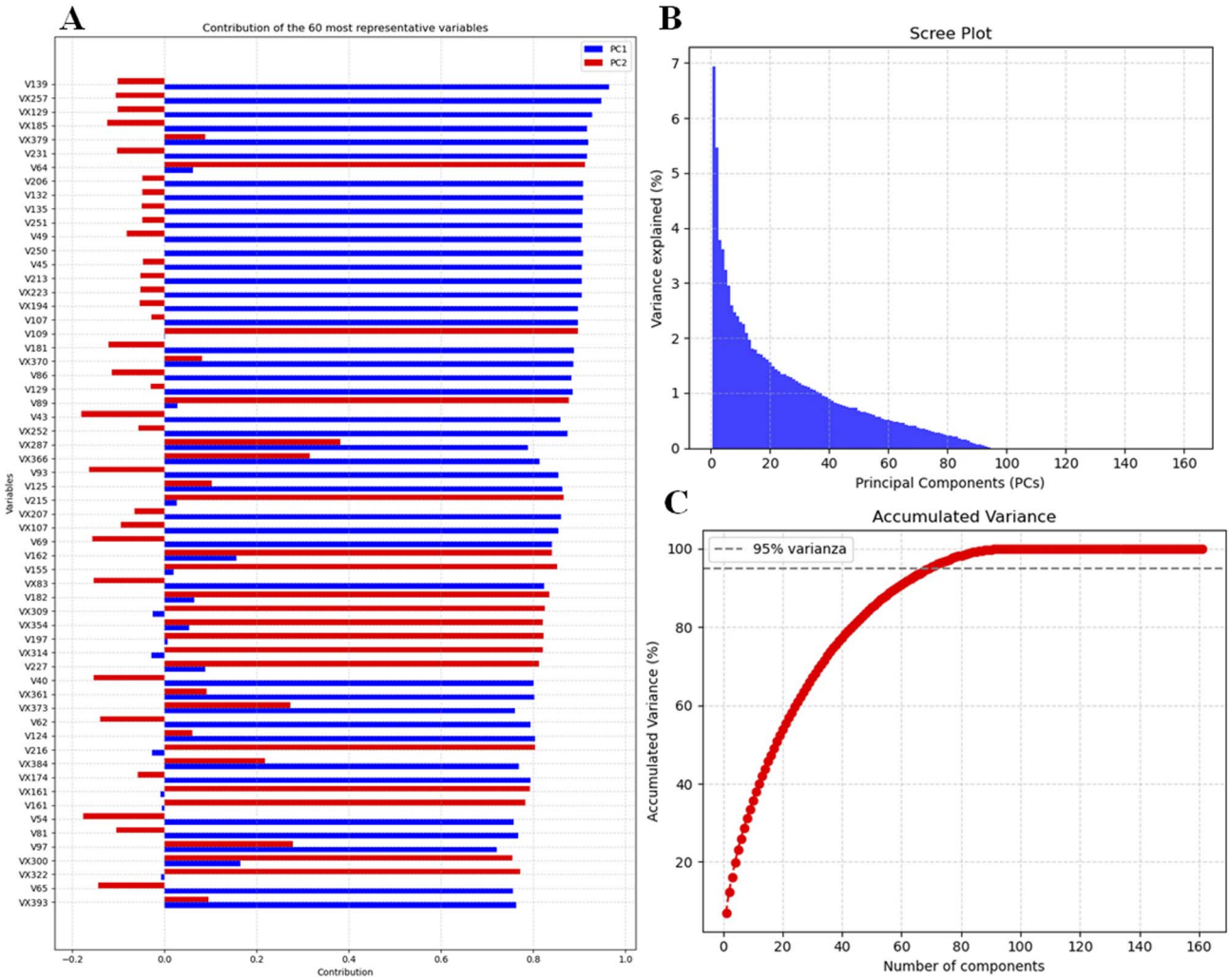

Fig. 5 (A) Contribution of the most representative variables. (B) Variance explained by each principal component. (C) Cumulative variance analysis.

blue circles (undoped samples) and yellow crosses (treated samples). The model shows that PLS1 accounts for 62.73% of the variance, while PLS2 explains 7.27%, indicating a clear separation between the two groups and confirming that the PLS-DA model effectively discriminates between doped and undoped samples. Additionally, no overlapping of samples is observed, reinforcing the hypothesis of a significant biological effect induced by endosulfan as a xenobiotic agent. Based on the PLS-DA results, the 30 most important variables (VIP) contributing to the separation between groups within the model were identified (Fig. 6C).

The determination of VIP scores generated from the PLS-DA model indicated that variables with VIP > 1.0 are considered relevant for classification; however, for this study, only those with VIP > 3.0 were selected, identifying V13, V3, V54, and V29 as the most discriminatory metabolites within the model. To verify these results, cross-validation was performed, yielding an optimal classification threshold of 0.9251 and a PLS-DA model accuracy of 0.75.

Given this moderate accuracy, the data were further evaluated using a random forest model, which generated a balanced working subset for the class groups. Cross-validation of this model achieved an accuracy of 1.00, demonstrating that this method efficiently classifies doped and undoped samples. VIP scores were then determined from the random forest model (Fig. 7A), with variables having VIP > 0.025 considered significant. The most important contributors to the group differentiation were identified as VX83, V29, V54, V102, V13, V86, V129, and V3. Consistently, both the random forest and PLS-DA models identified V13, V3, and V54 as influential variables in discriminating between doped and undoped sample groups. To further evaluate the potential of these compounds as toxicity biomarkers, ROC and corrected AUC-ROC analyses were performed (Fig. 7B) to assess the individual predictive capacity of each variable. The results obtained from the corrected ROC-AUC analysis (Fig. 7B) indicate that the metabolites V93, V129, V86, V102, V29, V54, V57, V13, V139, V218, V43, V3, and V1, along with the unidentified signals VX83, VX130, and VX281,

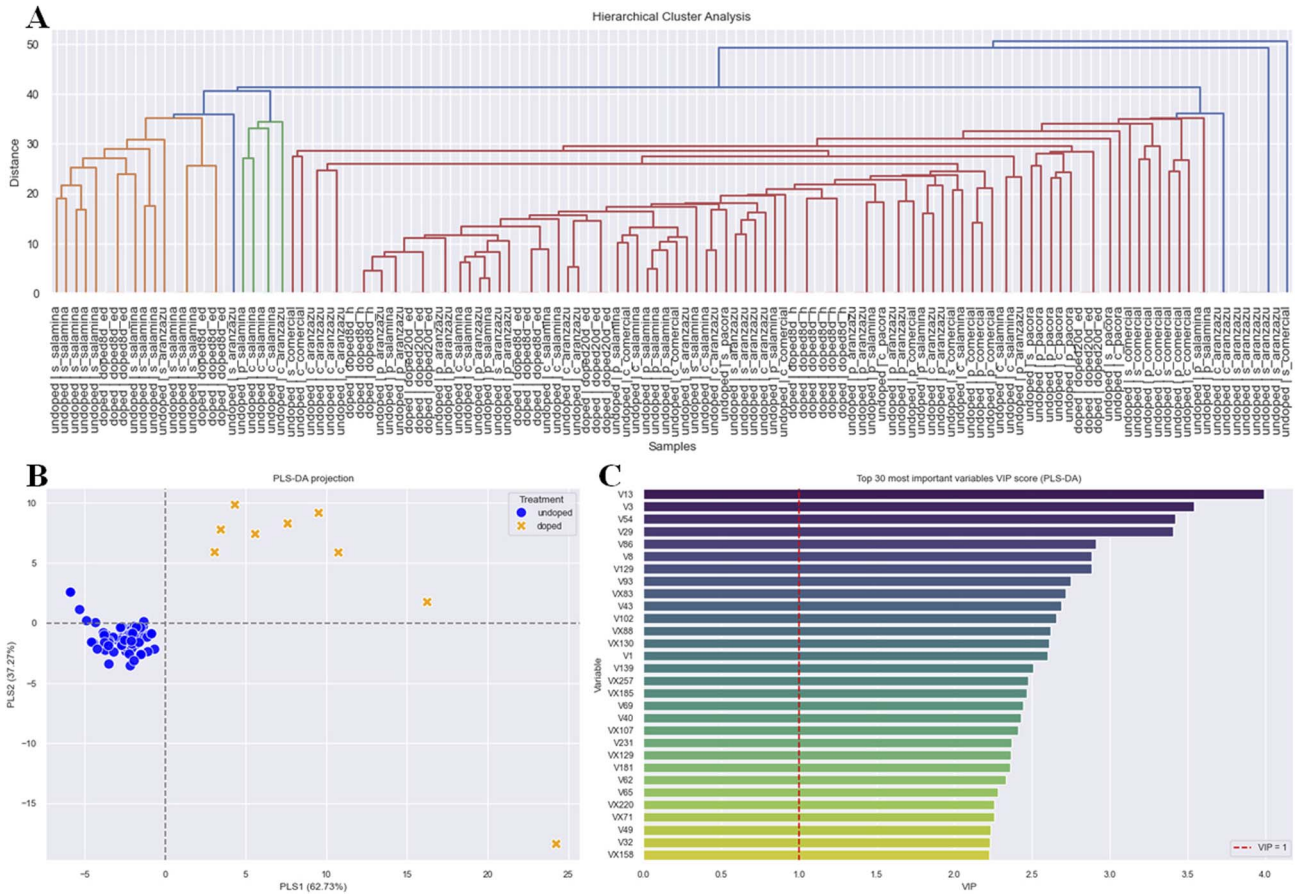

Fig. 6 (A) Hierarchical cluster analysis (HCA). (B) Partial least squares discriminant analysis (PLS-DA). (C) Top variable importance in projection (VIP) scores generated from the PLS-DA model.

can be considered volatile organic compounds (VOCs) with potential as toxicity biomarkers for the preventive detection of xenobiotic agents, such as endosulfan, in Hass avocado crops.

3.4 Potential toxicity biomarkers

To determine potential toxicity biomarkers, the Mann–Whitney (U) statistical test was applied to assess the significance of the listed 16 variables as potential biomarkers. This test showed that these selected variables can indeed be considered potential toxicity biomarkers.

The p-values for this test were calculated using a custom Python script (version 3.13.5), specifically employing the scipy.stats library. However, to confirm this information, an ROC curve analysis was conducted for all 16 variables (Table 3). In

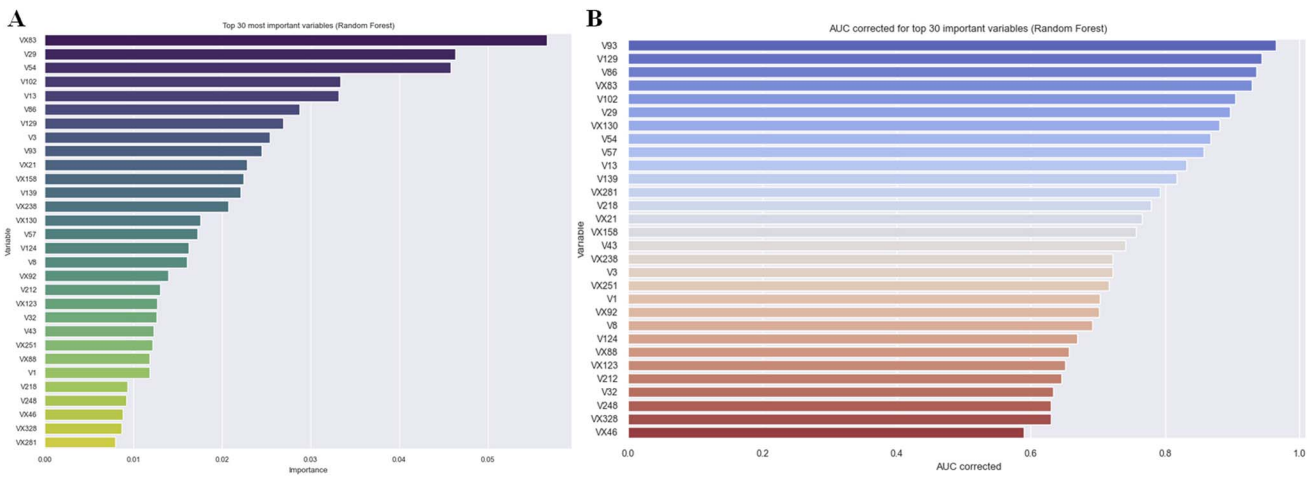

Fig. 7 (A) Principal VIPs generated from the random forest. (B) VIPs related to the corrected AUC.

Table 3 Candidate response metabolites as potential toxicity biomarkers in Hass avocado

Compound number	Code	Compound	*U* statistic (Mann–Whitney)	*p*-Value	Curve ROC-AUC	Potential biomarker of toxicity (significance)
1	V93	(*E*)-2-Octenal	2580.00	0.0000	0.97	**
2	V129	Decanal	2523.00	0.0000	0.94	**
3	V86	Oct-3-en-2-one	2500.50	0.0000	0.94	**
4	V102	Nonanal	2418.00	0.0000	0.90	**
5	V29	Hexanal	2395.50	0.0000	0.90	**
6	V54	(*E*)-2-Heptenal	2319.00	0.0000	0.87	*
7	V57	Benzaldehyde	2290.50	0.0000	0.86	*
8	V13	Hexane, 2,2-dimethyl-	2223.00	0.0000	0.83	*
9	V139	(*E*)-2-Decenal	2182.50	0.0000	0.82	*
10	V218	Zonarene	2083.50	0.000	0.78	*
11	V43	Heptanal	1980.00	0.000	0.74	*
12	V3	Acetonitrile	1930.50	0.0000	0.72	*
13	V1	Methyl isocyanide	1878.00	0.0000	0.70	*
14	VX83	—	2484.00	0.0000	0.93	**
15	VX130	—	2355.00	0.0000	0.88	*
16	VX281	—	2118.00	0.0000	0.79	*

** Acceptance criterion for ROC-AUC $\geq$ 0.90. (Ref 34). * Significance U stadistic (Mann-Whitney).

this way, metabolites with an ROC-AUC value $\geq$ 0.9 indicate a very high ability to correctly separate the two evaluated groups (doped and non-doped samples), suggesting that they can be considered effective potential toxicity biomarkers.

This study determined the ROC-AUC values for the 16 candidate biomarker compounds, of which the ROC-AUC curve indicates a superior or equal performance to 0.9 for the variables V93 (Fig. 8A), V129 (Fig. 8B), V86 (Fig. 8C), V102 (Fig. 8D), V29 (Fig. 8E), and an unknown metabolite categorized as VX83 (Fig. 8F). Therefore, these 6 compounds were identified as potential toxicity biomarkers, as they individually exhibit a strong ability to discriminate between the doped and non-doped sample groups in Hass avocado. To date, no previous studies have reported the identification of potential toxicity biomarkers in Hass avocado. However, studies have been reported on the exploration of physicochemical and metabolomic markers developed during the fruit's ripening process.[35]

Additionally, in the context of omics research in Hass avocado, genomic analyses have been employed to assess the genotoxicological effects of the ethanol extract obtained from the seed of this fruit.[36] Transcriptomic studies focus on identifying hormonal biomarkers to determine the physiological age of the fruit, as well as understanding the expressed biochemical changes. These studies have revealed the overexpression of genes associated with DNA replication, auxin transport, cell wall modifications, and the biosynthesis of gibberellins, brassinosteroids, and flavonoids.[37] Regarding proteomic studies, there is a comparative analysis between the peel and pulp, evaluating their shelf life after harvest.[38]

Most current research on this fruit focuses on exploring this matrix to identify bioactive compounds such as fatty acids present in the tissue, for antimicrobial purposes, food additive properties, and the identification and quantification of phytochemicals generated during the fruit's ripening stage.[40,41] In metabolomic studies, a combination of GC-MS and HPLC-UV-VIS techniques, based on chemometric methods, has been used to discriminate between Hass avocado samples that present and do not present physiological disorders such as black spot.[42] This indicates that this biological matrix has been extensively studied from an exploratory perspective to identify its biological and nutritional properties. Chemically, the fruit is characterized by the presence of alcohols, fatty acids, phenolic compounds, carotenoids, carbohydrates, furan derivatives and furanones, diterpenes, lignans, among others.[43] These compounds contribute to the nutritional value of this matrix and enhance its consumption, highlighting its potential. Therefore, the importance of the preventive determination of toxicological alterations in this fruit lies in this context. This study marks the beginning of the first xenovolatilomic research focused on identifying potential toxicity biomarkers, expressed through the controlled exposure of endosulfan to the peel, pulp, and seed of Hass avocado, with exposure periods of 8 and 20 days, respectively.

3.5 Metabolic pathways

3.5.1 Biochemical pathway enrichment analysis. The biological understanding of the metabolites identified in the peel, pulp, and seed of Hass avocado, exposed to endosulfan, required a pathway enrichment analysis using the MetaboAnalyst platform (Fig. 9).

This analysis aimed to identify the involvement of pathways such as: pyruvate metabolism ($p = 0.0032856$, $-\log(p) = 2.4834$, Holm $p = 0.30556$, impact = 0.03409), glycolysis or gluconeogenesis ($p = 0.0041979$, $-\log(p) = 2.377$, Holm $p = 0.3862$, impact = 0.03155), fatty acid biosynthesis ($p = 0.01884$, $-\log(p) = 1.7249$, Holm $p = 1.0$, impact = 0.01123), sesquiterpenoid and triterpenoid biosynthesis ($p = 0.0435$, $-\log(p) = 1.3615$, Holm $p = 1.0$, impact = 0.0), phenylalanine metabolism ($p = 0.047375$, $-\log(p) = 1.3244$, Holm $p = 1.0$, impact = 0.0), cutin,

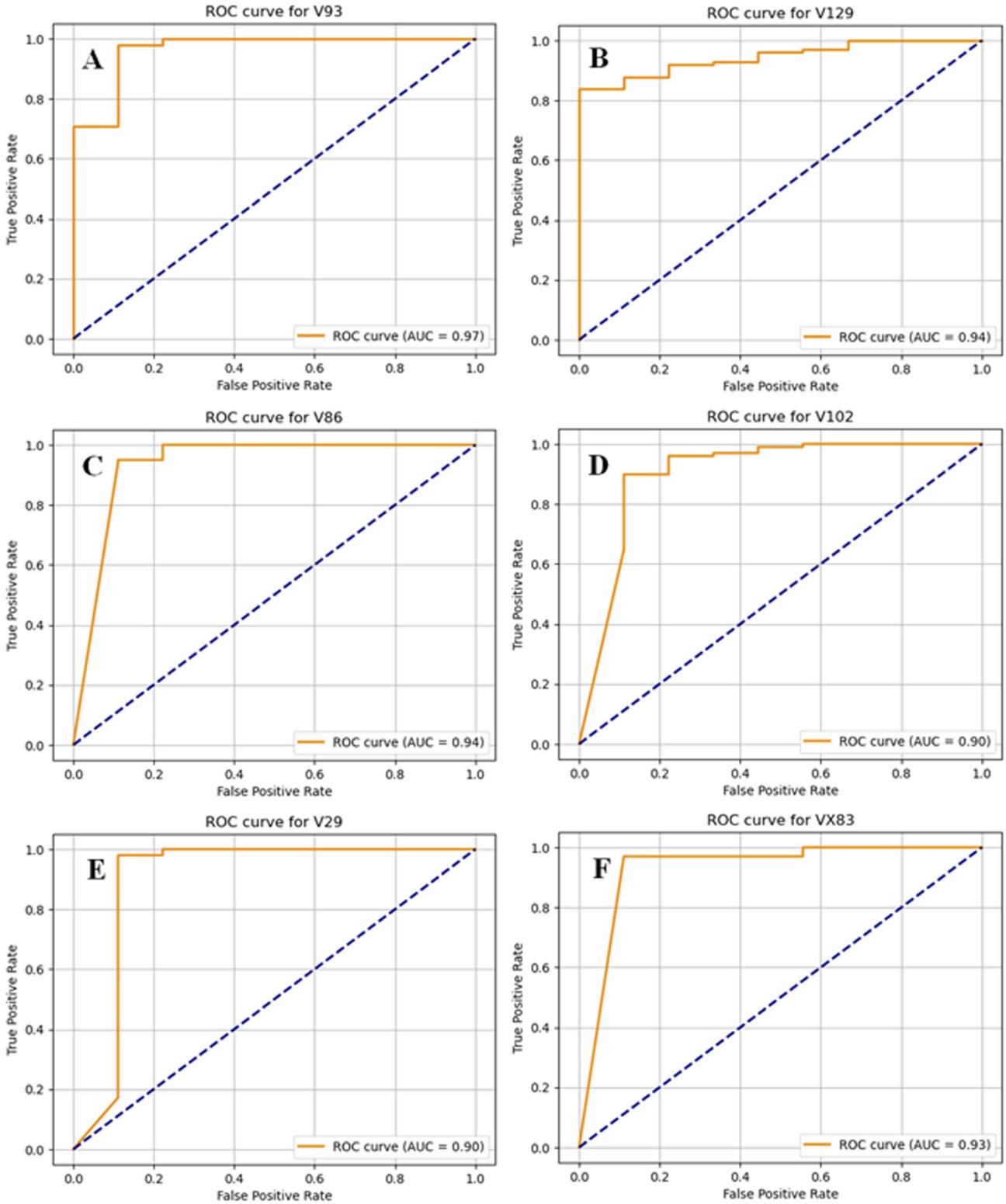

Fig. 8 AUC-ROC curves for the following compounds: (A) V93 ((*E*)-2-Octenal). (B) V129 (Decanal).[39] (C) V86 (Oct-3-en-2-one). (D) V102 (Nonanal).[39] (E) V29 (Hexanal).[39] (E) V29 (Hexanal).[39] (F) VX83 (unknown compound).

suberin and wax biosynthesis ($p = 0.070352$, $-\log(p) = 1.1527$, Holm $p = 1.0$, impact $= 0.0$), biosynthesis of unsaturated fatty acids ($p = 0.085412$, $-\log(p) = 1.0685$, Holm $p = 1.0$, impact $= 0.0$), fatty acid elongation ($p = 0.089145$, $-\log(p) = 1.0499$, Holm $p = 1.0$, impact $= 0.0$), glycosylphosphatidylinositol (GPI)-anchor biosynthesis ($p = 0.10762$, $-\log(p) = 0.96811$, Holm $p =$

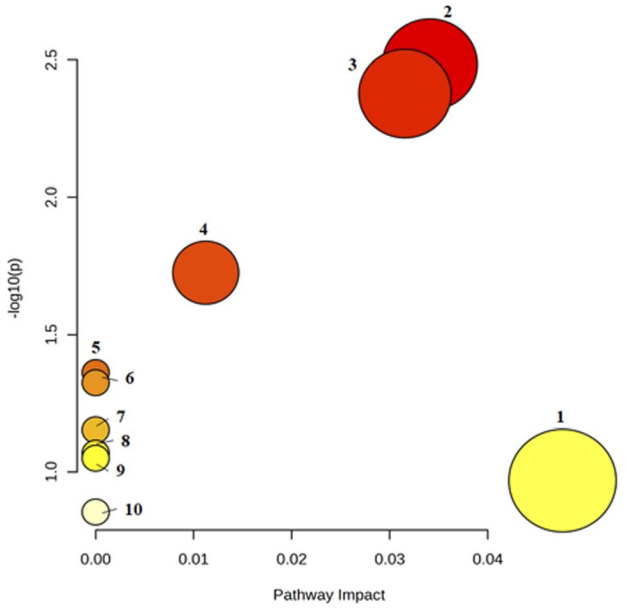

Fig. 9 Results of the pathway enrichment analysis. (1) Glycosylphosphatidylinositol (GPI)-anchor biosynthesis. (2) Pyruvate metabolism. (3) Glycolysis or gluconeogenesis. (4) Fatty acid biosynthesis. (5) Sesquiterpenoid and triterpenoid biosynthesis. (6) Phenylalanine metabolism. (7) Cutin, suberin and wax biosynthesis. (8) Biosynthesis of unsaturated fatty acids. (9) Fatty acid elongation. (10) Fatty acid degradation.

1.0, impact = 0.0), fatty acid degradation ($p = 0.14009$, $-\log(p) = 0.8536$, Holm $p = 1.0$, impact = 0.0).

3.5.2 Biochemical alteration of the peel, pulp, and seed in Hass avocado. Fig. 10A and B show the metabolic pathways constructed from the KEGG (blue), HMDB (purple), Lipid Maps (orange), and MetaCyc (brown) databases, representing the metabolites in these colors and the different enzymes involved in these processes in red. The biochemical pathways associated with the various metabolites present in the biosynthesis process of these compounds are represented in green. In Fig. 10A, a lower density of connections and a limited number of activated pathways are observed through the expression of response metabolites in the peel following endosulfan exposure, highlighting the activation of pathways such as: phospholipid pathway, toluene degradation, lipid metabolism, monoterpenoid biosynthesis, fatty acid biosynthesis, sphingolipid pathway, sesquiterpenoid and triterpenoid biosynthesis. Therefore, biologically, the activation of these biochemical pathways suggests an initial response to oxidative stress caused by endosulfan, where chemical species are generated from lipid metabolism. On the other hand, in Fig. 10B, the participation of biochemical pathways such as lipid metabolism, toluene degradation, sphingolipid pathway, phospholipid pathway, lipid biosynthesis, fatty acid biosynthesis, sesquiterpenoid and triterpenoid biosynthesis, and the Krebs cycle (TCA cycle) is observed.

This indicates the activation of lipid oxidation pathways, leading to the production of oxylipins,[44] and other lipid peroxidation products as oxidative damage progresses under endosulfan exposure. As the exposure time increases, metabolic dysregulation intensifies, resulting in the biosynthesis and accumulation of specific potential toxicity biomarkers. In this study, five volatile compounds were identified as key biomarkers: (*E*)-2-octenal (V93), oct-3-en-2-one (V86), decanal (V129), nonanal (V102), and hexanal (V29). These VOCs are directly associated with unsaturated fatty acid degradation and lipid peroxidation, processes exacerbated by the inhibition of detoxification enzymes affected by endosulfan, making them reliable indicators of xenobiotic-induced oxidative stress in Hass avocado.

In Fig. 11A, a lower density of connections between the metabolites identified in the pulp is observed after an 8 day exposure to endosulfan. This exposure process induces the alteration of pathways such as lipid metabolism, phospholipid pathway, sphingolipid pathway, fatty acid biosynthesis, and toluene degradation. It can be observed that, at this early stage, endosulfan begins to cause lipid alterations and degradation pathways of VOCs, but no massive disruption occurs in the pulp of the Hass avocado yet. After 20 days (Fig. 11B), a higher density of connections between metabolites and biochemical pathways is observed, such as lipid metabolism, sphingolipid pathway, furfural degradation, toluene degradation, phospholipid pathway, and fatty acid biosynthesis. A greater number of enzymes involved in the biochemical alteration processes is observed, indicating that endosulfan causes significant disruption in lipid homeostasis and other pathways for aldehyde degradation. This explains the increase in analytical signals of compounds like hexanal, as the accumulation of the xenobiotic is biochemically enhanced, inhibiting key enzymes and inducing lipoperoxidation processes and degradation of unsaturated fatty acids, leading to the formation and increase in the number of aldehyde-type compounds.

For the case of the seed, Fig. 12A shows a similar trend to the metabolite connection network in the peel and pulp. Identifying, at an 8 day exposure period, few connections between biochemical pathways and metabolites, with the activation of pathways such as: TCA cycle, toluene degradation, lipid metabolism, monoterpenoid biosynthesis, lipid biosynthesis, sesquiterpenoid and triterpenoid biosynthesis, phospholipid pathway, pinene, camphor and geraniol degradation, and fatty acid biosynthesis. Based on the involvement of these biochemical pathways, an initial response to endosulfan toxicity is evident, primarily affecting lipid metabolism and the degradation of monoterpenes and sesquiterpenes. This suggests the induction of oxidative processes, as these pathways are associated with an early stage of metabolic stress and cellular adaptation. At 20 days of exposure in the seed (Fig. 12B), interaction with endosulfan leads to the activation of biochemical pathways such as: sphingolipid pathway, furfural degradation, pinene, camphor and geraniol degradation, phenylalanine metabolism, lipid biosynthesis, toluene degradation, sesquiterpenoid and triterpenoid biosynthesis, phospholipid pathway, fatty acid biosynthesis, TCA cycle, and lipid metabolism. The number of implicated biochemical pathways increases, with the additional involvement of the phenylalanine metabolism pathway. Furthermore, it is observed that after 20 days of exposure, there is a marked intensification of lipid and

oxidative degradation, activating aromatic detoxification pathways, increasing enzymatic participation, and revealing a systemic disturbance affecting critical metabolic routes. This process drives Hass avocado into a state of generalized metabolic stress, amplifying enzymatic activity and triggering the opening of new detoxification and degradation pathways.[45]

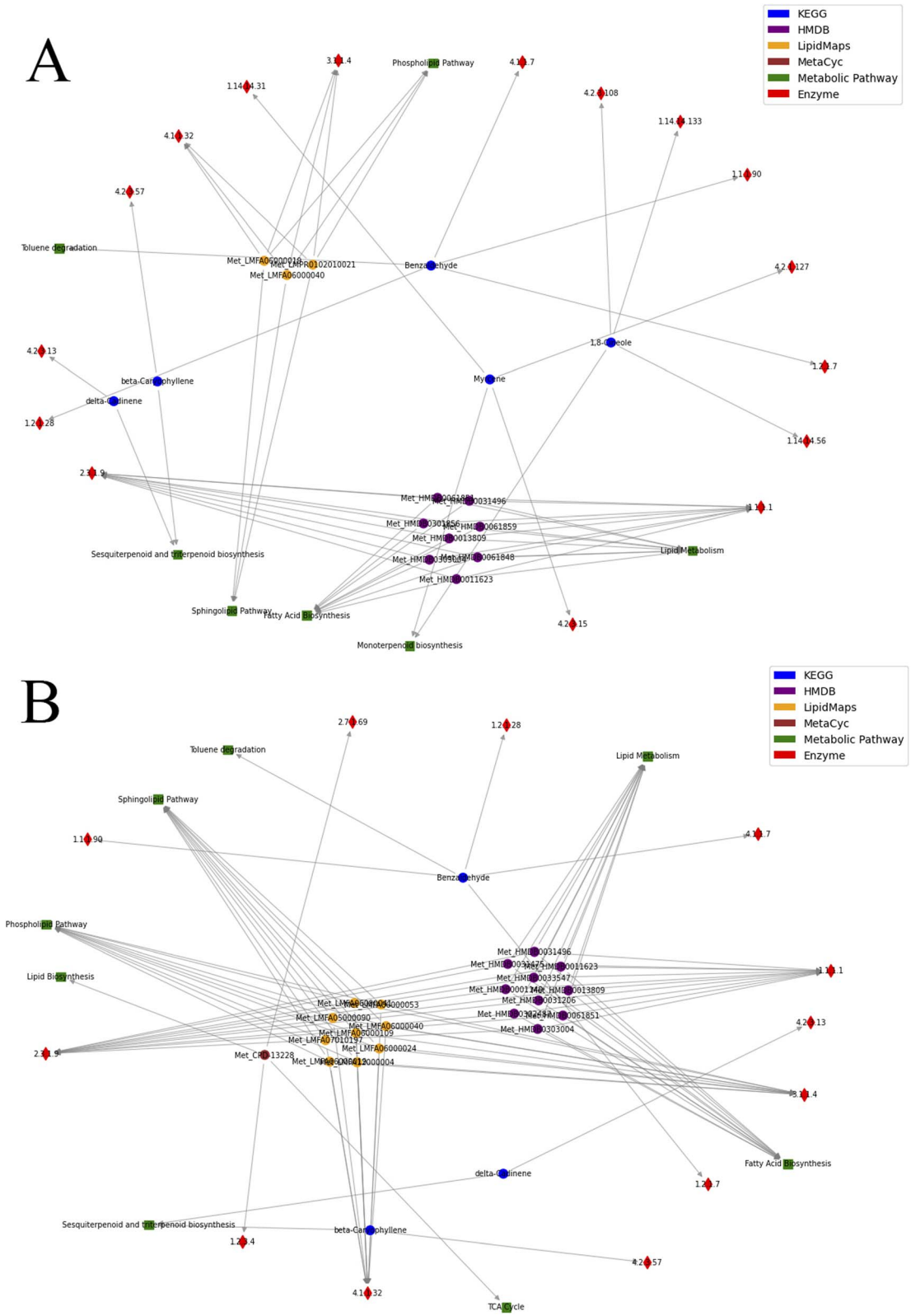

Fig. 10 (A) Biochemical pathways identified in the xenovolatilomic profile for Hass avocado peel during an 8 day exposure period. (B) Biochemical pathways identified in the xenovolatilomic profile for Hass avocado peel during a 20 day exposure period.

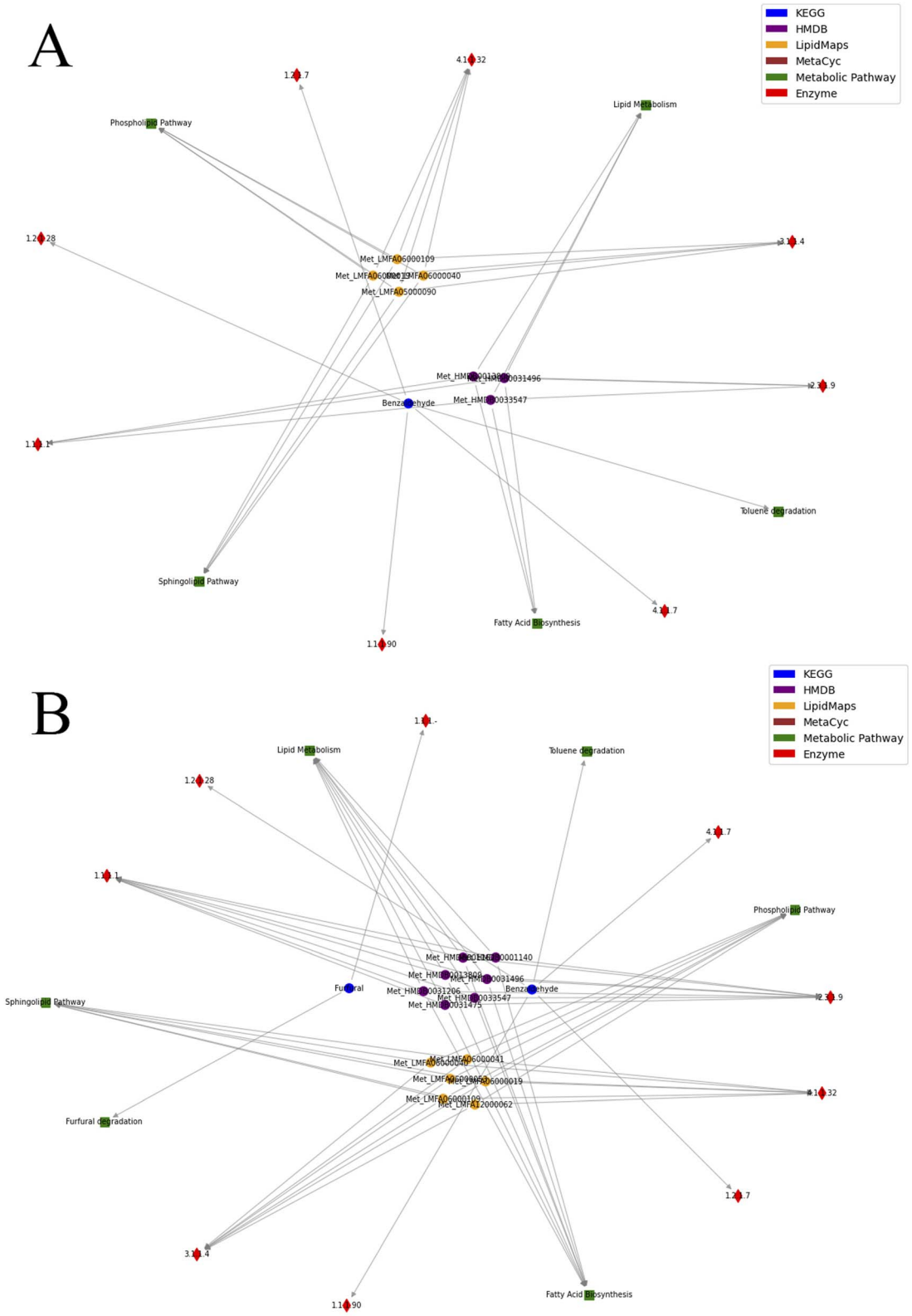

Fig. 11 (A) Biochemical pathways identified in the xenovolatilomic profile of Hass avocado pulp after an 8 day exposure period. (B) Biochemical pathways identified in the xenovolatilomic profile of Hass avocado pulp after a 20 day exposure period.

3.5.3 Biosynthesis of toxicity biomarkers. (*E*)-2-Octenal is part of the biochemical pathway involved in the oxidative degradation of unsaturated fatty acids. Decanal is produced through the β-oxidation of long-chain fatty acids, while oct-3-en-2-one is generated from lipid degradation and ketone oxidation. Nonanal is formed *via* the oxidation of unsaturated fatty acids,

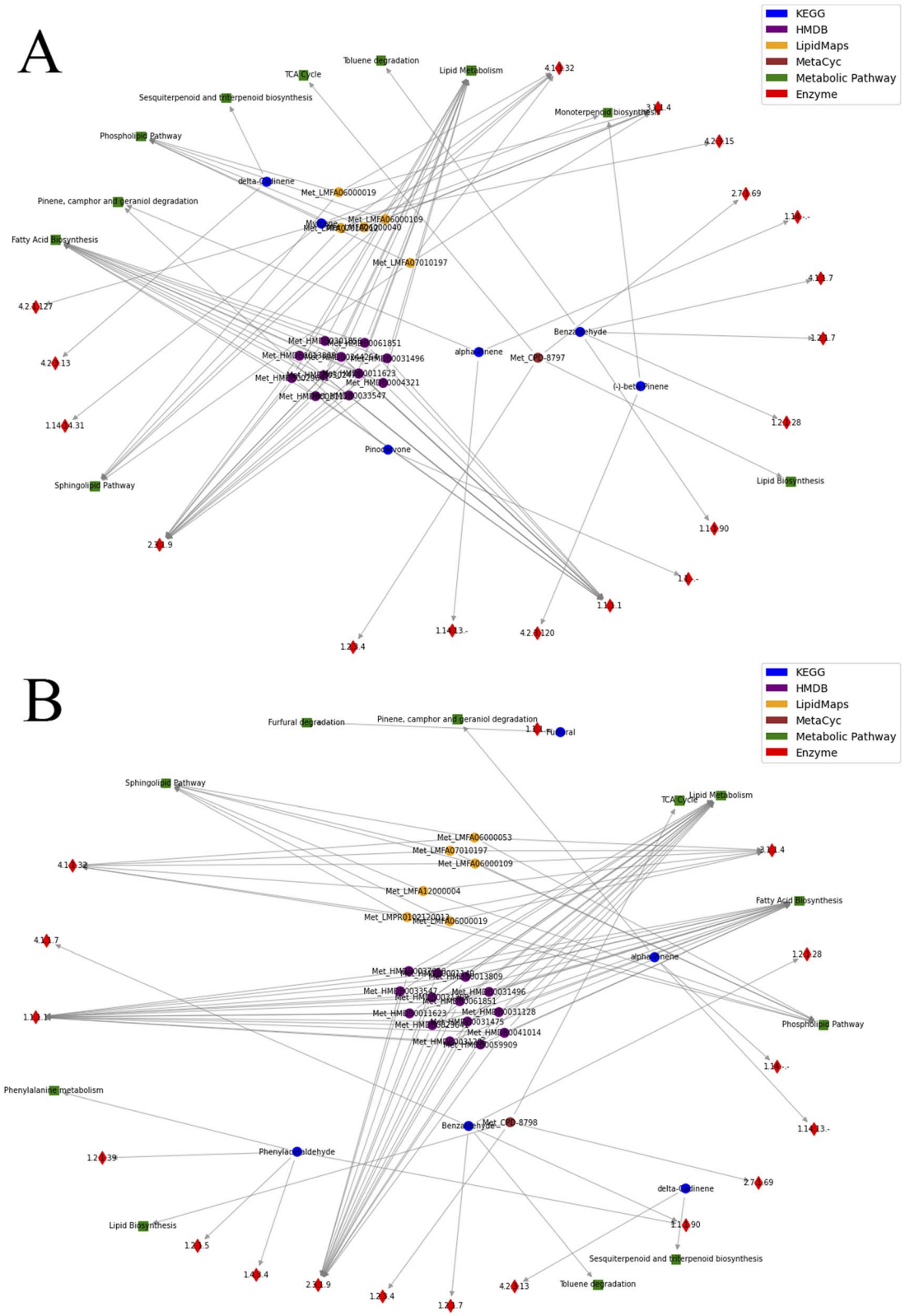

Fig. 12 (A) Biochemical pathways identified in the xenovolatilomic profile of Hass avocado seed after an 8 day exposure period. (B) Biochemical pathways identified in the xenovolatilomic profile of Hass avocado seed after a 20 day exposure period.

and hexanal is produced through the lipoxygenation of polyunsaturated fatty acids. The accumulation of these potential toxicity biomarkers reflects a sustained oxidative stress response induced by endosulfan exposure. Endosulfan disrupts lipid metabolism by inhibiting key detoxification enzymes such as cytochrome P450 monooxygenases, aldehyde

dehydrogenases, and lipoxygenases, impairing the normal catabolism of lipid peroxidation products. This enzymatic inhibition leads to the progressive buildup of oxidized lipid derivatives, which serve as chemical indicators of cellular damage under prolonged xenobiotic stress.

This lipophilic organochlorine pesticide is a known inhibitor of several key enzymes, including cytochrome P450 monooxygenases (CYPs)—essential for lipid metabolism, aldehyde dehydrogenases (ALDH)—which convert toxic aldehydes into carboxylic acids, lipoxygenases (LOX)—catalysts in the oxidation of polyunsaturated fatty acids and the formation of hydroperoxides,[46] alcohol dehydrogenases (ADH)—involved in converting alcohols into aldehydes, fatty acid synthase (FAS) enzymes—which drive the development of precursor compounds for oxylipins and aldehydes, and peroxisomal enzymes such as acyl-CoA oxidase and catalase—both affected by the accumulation of free radicals, and involved in the β-oxidation of fatty acids.[47]

The inhibition of these enzymes leads to the accumulation of oxidized lipids,[48] further enhancing lipid peroxidation and promoting the formation of VOCs such as hexanal, (*E*)-2-octenal, and nonanal. These compounds serve as chemical signals that reflect the plant's—and specifically the fruit's—response to chemical stress caused by environmental contaminants like endosulfan.[49] The production of these compounds exacerbates mitochondrial dysfunction, favoring pathways such as fatty acid biosynthesis, sphingolipid metabolism, and the lipoxygenase (LOX) pathway.[50] As a result, a specific distribution of the affected enzymes and their metabolic impact can be observed in each part of the fruit. In the peel, enzymes such as CYPs, LOX, and ALDH are disrupted, leading to increased lipid peroxidation and the production of six- and nine-carbon aldehydes. In the pulp, enzymes like ADH, CYPs, and FAS are primarily affected, promoting the accumulation of aldehydes and ketones.[51] In the seed, the inhibition of CYPs, ALDH, and peroxisomal enzymes alters the deeper defense metabolism, causing the retention of aldehydes.[52]

Chemically, these toxicity biomarkers are formed through the lipoxygenase (LOX) and hydroperoxide lyase (HPL) pathway, which represents the main route for the generation of volatile aldehydes and ketones in plants, triggering the onset of lipid peroxidation.[53] Unsaturated fatty acids such as linoleic acid and oleic acid are oxidized by LOX to form fatty acid hydroperoxides. These hydroperoxides are subsequently cleaved by the action of HPL,[54] producing six- and ten-carbon aldehydes, some of which can undergo isomerization, as in the case of (*E*)-2-octenal, or be reduced to their corresponding alcohols.

Additionally, β-oxidation in peroxisomes contributes to the formation of intermediate compounds such as medium-chain aldehydes and ketones. These biomarkers are involved in plant defense pathways against pathogens or oxidative stress induced by xenobiotic agents.[55] Furthermore, they participate in the biochemical routes responsible for fruit aroma and flavor, modulating organoleptic properties, plant signaling processes, and lipid oxidation.[56] Table 4, presents the codes of the main enzymes involved in the biochemical alterations induced by endosulfan, along with selected representations of crystalline structures reported in the Protein Data Bank (PDB), providing

Table 4 Enzymes involved in the biochemical alteration process of peel, pulp, and seed of Hass avocado

Enzymes	EC code	Main function	Example representative PDB entry	Species
Cytochrome P450 monooxygenase (CYP)	EC 1.14.-.-	Oxidation of organic compounds by the incorporation of an oxygen atom	6L8H	*Arabidopsis thaliana* (Cytochrome P450) [57]
Aldehyde dehydrogenase (ALDH)	EC 1.2.1.3	Oxidation of aldehydes to carboxylic acids using NAD^+/NADH as cofactor	4PXL	*Zea mays*[58]
Lipoxygenase (LOX)	EC 1.13.11.12	Oxidation of polyunsaturated fatty acids to form hydroperoxides	1IK3	*Glycine max*[59]
Alcohol dehydrogenase (ADH)	EC 1.1.1.1	Reversible conversion of alcohols to aldehydes or ketones using NAD^+/NADH	1YQD	*Populus tremuloides*[60]
Fatty acid synthase (FAS)	EC 2.3.1.85	Synthesis of long-chain fatty acids from acetyl-CoA and malonyl-CoA	2IX4 1W0I	*Arabidopsis thaliana*[61,62]
Acetyl-CoA carboxylase (ACC)	EC 6.4.1.2	Carboxylation of acetyl-CoA to form malonyl-CoA, a key step in lipogenesis	1OD4	*Saccharomyces cerevisiae*[63,64]
Acyl-CoA oxidase	EC 1.3.3.6	Oxidation of acyl-CoA to *trans*-2-enoyl-CoA in the β-oxidation of fatty acids	1W07	*Arabidopsis thaliana*[65]
Catalase	EC 1.11.1.6	Decomposition of hydrogen peroxide into water and oxygen, protecting against oxidative stress	1 A4E	*Saccharomyces cerevisiae*[66]

a basis for future computational metabolomics research applied to these plant enzymes.

This study makes a pioneering contribution to the emerging field of xenovolatilomics by identifying a series of volatile organic compounds as potential toxicity biomarkers in Hass avocado following pesticide exposure. The identification of (*E*)-2-octenal, oct-3-en-2-one, decanal, hexanal,[67] and nonanal provides a solid foundation for future development of rapid diagnostic tools aimed at detecting agrochemical contamination. Moreover, the study underscores the tissue-specific enzymatic disruptions caused by xenobiotics like endosulfan, offering a novel plant-based model for investigating stress-induced metabolic responses.[68]

It is important to highlight that currently, only a limited number of crystallized and isolated enzymes from *Persea americana* are available in the Protein Data Bank (PDB). As a result, the enzymatic structures referenced in this study are drawn from representative plant and model species such as *Saccharomyces cerevisiae*, *Arabidopsis thaliana*, *Populus tremuloides*, *Glycine max*, and *Zea mays*. These examples provide a valuable biochemical framework and serve as analogs for future applications in computational metabolomics and enzyme modeling in non-model tropical crops like Hass avocado. Establishing these foundational comparisons may foster new research pathways in structural enzymology and strengthen predictive insights into xenobiotic interactions within food systems.

4 Conclusions

This study makes a significant contribution to the advancement of omics sciences, particularly within the field of volatilomics, by reporting the first xenovolatilomic investigation in Hass avocado (*Persea americana* Mill.), and the first study focused on the identification of potential toxicity biomarkers in this species from the Department of Caldas, Colombia. The structural identification and statistical validation of five key volatile compounds—(*E*)-2-octenal (V93), decanal (V129), oct-3-en-2-one (V86), nonanal (V102), and hexanal (V29)—support their role as potential toxicity biomarkers for the early detection of pesticide-induced biochemical alterations. These findings were validated through multivariate statistical approaches, including PLS-DA, random forest, VIP scoring, ROC curve, and AUC-ROC analyses, and were biochemically supported by the identification of an oxidative stress response triggered by endosulfan. This stress was linked to the inhibition of key enzymes involved in fatty acid and aldehyde metabolism, resulting in the accumulation of the identified VOCs.

In addition, this work established the biochemical context for the formation of these biomarkers by identifying key enzymatic targets, listing their respective EC codes, and providing representative crystal structures reported in the Protein Data Bank (PDB). This biochemical mapping lays the foundation for future research, including the development of validation models for toxicity biomarkers and the application of computational metabolomics to predict enzyme inhibition patterns induced by xenobiotics.

Importantly, the unknown compound VX83 was tentatively identified as 4-pentenal, with a similarity index (SI) of 83%, highlighting its potential as a novel biomarker pending full structural and functional elucidation. Moreover, this study emphasizes the relevance of response metabolites formed under xenobiotic stress, which serve as additional indicators of biochemical disruption. The xenovolatilomic profile revealed previously unreported VOCs in Hass avocado tissues, including 2-heptanone (V40), cyclohexanecarboxaldehyde (V49), octyl acetate (V132), veratrole (V111), dipentyl ketone (V140), and 1,9-decadiene (V142)—each contributing to the overall stress signature associated with endosulfan exposure. Overall, this research successfully integrates xenovolatilomic profiling with statistical and biochemical modeling, confirming the reliability of these VOCs as toxicity indicators. It also demonstrates temporal metabolic differentiation (8 *vs.* 20 days of exposure), and addresses critical challenges in the early detection of emerging contaminants. These findings have direct implications for food quality monitoring, export compliance, and the long-term economic sustainability of avocado production systems in the Caldas region.

Data availability

The data supporting this article have been included as part of the ESI.†

Author contributions

JPBA: Manuscript preparation, methodology design, and statistical analysis. APO: Sample processing using GC-MS. JAFL: Validation of the obtained data. GTO: Writing, review, and editing of the final document.

Conflicts of interest

The authors declare that they have no conflict of interest with respect to the content of this article.

Acknowledgements

The authors would like to thank the Ministry of Science, Technology, and Innovation for the support provided through Call 907: "Call for Young Researchers and Innovators within the Framework of Economic Reactivation 2021". We also extend our gratitude to the Vice-Rectory for Research and Postgraduate Studies at the University of Caldas, and to the Research Group in Chromatography and Related Techniques for their valuable support.

References

1 J. S. Ramírez-Navasa, F. Jaramillo-López and L. López, Las disciplinas ómicas en la ciencia de los alimentos, *Revista Colombiana De Investigaciones Agroindustriales*, 2023, vol. 10(2), pp. 1–22, DOI: 10.23850/24220582.5694.

2 K. Panchal, K. Murjani and V. Singh, *Current Approaches on Metabolomics*, 2024, pp. 1–14, DOI: 10.1007/978-981-97-7459-3_1.
3 J. P. Betancourt-Arango, E. E. Villaroel-Solis, J. A. Fiscal-Ladino and G. Taborda-Ocampo, Volatilomics: an emerging discipline within omics sciences – a systematic review, *F1000Research*, 2024, **13**, 991, DOI: 10.12688/f1000research.149773.1.
4 C. Carazzone, J. P. G. Rodríguez, M. Gonzalez and G. D. López, Volatilomics of Natural Products: Whispers from Nature, Metabolomics – Methodol, *Appl. Med. Sci. Life. Sci.*, 2021, DOI: 10.5772/intechopen.97228.
5 A. Olander, C. A. Lawson, M. Possell, J. B. Raina, M. Ueland and D. J. Suggett, Comparative volatilomics of coral endosymbionts from one- and comprehensive two-dimensional gas chromatography approaches, *Mar. Biol.*, 2021, **168**(5), 1–13, DOI: 10.1007/s00227-021-03859-2.
6 J. P. Betancourt-Arango, A. Patiño-Ospina, G. Taborda-Ocampo and J. A. Fiscal-Ladino, Aplicaciones de la xenometabolómica para la identificación de biomarcadores de toxicidad: una revisión del tema, *Biosalud*, 2025, **19**(1), 7–30, DOI: 10.17151/biosa.2020.19.1.1.
7 Q. Wei, H. Cui, Y. Hu, J. Li, S. Yue, C. Tang, Q. Zhao, Y. Yu, H. Li, Y. Qin, Y. Yang and J. Zhang, Comparative characterization of Taihe silky chicken and Cobb chicken using LC/MS-based lipidomics and GC/MS-based volatilomics, *LWT*, 2022, **163**, 113554, DOI: 10.1016/j.lwt.2022.113554.
8 N. Joguet, L. Jing, F. Jamois and P. Dumargue, Characterization of Volatile Organic Compounds (VOCs) from Farms Effluents: Interest of HS-SPME-GC-MS Technique for Laboratory and Field Test, *Atmosphere*, 2023, **14**(6), 928, DOI: 10.3390/atmos14060928.
9 M. Elizalde-González and E. Segura-Rivera, Volatile compounds in different parts of the fruit *Psidium guajava* L. cv. "Media China" identified at distinct phenological stages using HS-SPME-GC-QTOF/MS, *Phytochem. Anal.*, 2018, **29**, 649–660, DOI: 10.1002/pca.2778.
10 A. Raza, H. Song, N. Begum, J. Raza, M. Iftikhar, P. Li and K. Li, Direct Classification of Volatile Organic Compounds in Heat-Treated Glutathione-Enriched Yeast Extract by Headspace-Gas Chromatography-Ion Mobility Spectrometry (HS-GC-IMS), *Food Anal. Methods*, 2020, **13**(12), 1–11, DOI: 10.1007/s12161-020-01847-8.
11 K. Zanella, C. Lima Pinheiro, E. Tomaz and O. Taranto, Study of Volatiles from "Pera" Sweet Orange Peel Using Karl Fischer Titration, GC-FID and GC/MS Techniques, *Chem. Eng. Trans.*, 2013, **32**, 409–414, DOI: 10.3303/CET1332069.
12 A. Aminianfar, M. Fatemi and F. Azimi, Comprehensive characterization of volatile compounds in Iranian black teas using chemometric analysis of GC-MS fingerprints, *Food Chem.: X*, 2024, **24**(112), 101859, DOI: 10.1016/j.fochx.2024.101859.
13 M. Noshad, B. A. Behbahani and I. K. Karabagias, Volatilomic with chemometrics: a toward authentication approach for food authenticity control, *Eur. Food Res. Technol.*, 2023, **249**(9), 2215–2226, DOI: 10.1007/s00217-023-04291-0.
14 R. Chandra, N. Sharpanabharathi, B. A. K. Prusty, P. A. Azeez and R. M. Kurakalva, Organochlorine pesticide residues in plants and their possible ecotoxicological and agri food impacts, *Sci. Rep.*, 2021, **11**(1), 1–9, DOI: 10.1038/s41598-021-97286-4.
15 K. B. Githaiga, S. M. Njuguna, J. L. Bargul, F. Liu, R. W. Gituru and X. Yan, Decadal assessment of microplastics, pharmaceuticals, and pesticides as contaminants of emerging concerns (CECs) in Kenya's surface waters, a review, *Environ. Toxicol. Chem.*, 2023, **42**(10), 2105–2118, DOI: 10.1002/etc.5707.
16 P. K. Gupta and R. C. Gupta, Pharmacology, toxicology and degradation of endosulfan. A review, *Toxicology*, 1979, **13**(2), 115–130, DOI: 10.1016/S0300-483X(79)80016-5.
17 I. Sheriff, S. A. Debela and A. Mans-Davies, The listing of new persistent organic pollutants in the Stockholm convention: its burden on developing countries, *Environ. Sci. Policy*, 2022, **130**, 9–15, DOI: 10.1016/j.envsci.2022.01.005.
18 S. Karn, A. Upadhyay and A. Kumar, Biomonitoring of endosulfan toxicity in human, *Biocell*, 2022, **46**(7), 1771–1777, DOI: 10.32604/biocell.2022.018845.
19 J. Betancur, R. Ocampo and L. A Ríos, La problemática del endosulfán: aspectos químicos, analíticos y ambientales, *Luna Azul*, 2015, **40**, 293–313, DOI: 10.17151/10.17151/luaz.2015.40.19.
20 R. Muniyandi, Effect of Endosulfan on the Biodegradation and Bioaccumulation of Pesticides, *Asian J. Adv. Res.*, 2023, **6**(1), 150–160.
21 S. Rodríguez-Mozaz, A. Serra-Compte, R. Gil-Solsona and D. Álvarez-Muñoz, Environmental metabolomics and xenometabolomics for the assessment of exposure to contaminant mixtures, *Environ. Metabolomics*, 2020, 283–310, DOI: 10.1016/b978-0-12-818196-6.00010-8.
22 R. Gil-Solsona, D. Álvarez-Muñoz, A. Serra-Compte and S. Rodríguez-Mozaz, (Xeno)metabolomics for the evaluation of aquatic organism's exposure to field contaminated water, *Trends Environ. Anal. Chem.*, 2021, **31**, e00132, DOI: 10.1016/j.teac.2021.e00132.
23 G. Tan, Z. Lou, X. Dong, W. Li, W. Liao, Z. Zhu and Y. Chai, Urinary metabolites of isoliquiritigenin in wistar rats using UHPLC-TOF-MS-based xenometabolomics, *Chromatographia*, 2011, **74**(3), 341–348, DOI: 10.1007/s10337-011-2072-9.
24 J. P. Betancourt-Arango, C. A. Ossa-Jaramillo and G. Taborda-Ocampo, Extracción de plaguicidas en el aguacate Hass (*Persea americana* Mill. cv.) mediante el uso de C18 y arcillas funcionales como fase adsorbente en la metodología QuEChERS, *Rev. Acad. Colomb. Cienc. Exactas, Fis. Nat.*, 2021, **45**(174), 286–299, DOI: 10.18257/raccefyn.1235.
25 R. Feito, Y. Valcárcel and M. Catalá, Preliminary data suggest that venlafaxine environmental concentrations could be toxic to plants, *Chemosphere*, 2013, **90**(7), 2065–2069, DOI: 10.1016/j.chemosphere.2012.09.028.

26 A. H. Mahmoud, M. N. Samy, A. S. Wanas and M. S. Kamel, Gas chromatography-mass spectrometry profiling and analgesic, anti-inflammatory, antipyretic, and antihyperglycemic potentials of *Persea americana*, *Iran. J. Basic Med. Sci.*, 2021, **24**(5), 641–649, DOI: **10.22038/ijbms.2021.53390.12016**.

27 M. Wang, J. J. Carver, V. V. Phelan, L. M. Sanchez, N. Garg, Y. Peng, *et al.*, Sharing and community curation of mass spectrometry data with Global Natural Products Social Molecular Networking, *Nat. Biotechnol.*, 2016, **34**(8), 828–837, DOI: **10.1038/nbt.3597**.

28 M. Kanehisa, M. Furumichi, Y. Sato, M. Kawashima and M. Ishiguro-Watanabe, KEGG for taxonomy-based analysis of pathways and genomes, *Nucleic Acids Res.*, 2023, **51**(D1), D587–D592, DOI: **10.1093/nar/gkac963**.

29 J. Chong, D. S. Wishart and J. Xia, Using MetaboAnalyst 4.0 for Comprehensive and Integrative Metabolomics Data Analysis, *Curr. Protoc. Bioinf.*, 2019, **68**(1), 1–128, DOI: **10.1002/cpbi.86**.

30 C. Vicidomini, R. Palumbo, M. Moccia and G. N. Roviello, Oxidative Processes and Xenobiotic Metabolism in Plants: Mechanisms of Defense and Potential Therapeutic Implications, *J. Xenobiot.*, 2024, **14**(4), 1541–1569, DOI: **10.3390/jox14040084**.

31 F. Ramel, C. Sulmon, A. A. Serra, G. Gouesbet and I. Couée, Xenobiotic sensing and signalling in higher plants, *J. Exp. Bot.*, 2012, **63**(11), 3999–4014, DOI: **10.1093/jxb/ers102**.

32 M. A. Ahanger, N. A. Akram, M. Ashraf, M. N. Alyemeni, L. Wijaya and P. Ahmad, Plant responses to environmental stresses-from gene to biotechnology, *AoB Plants*, 2017, **9**(4), plx025, DOI: **10.1093/aobpla/plx025**.

33 M. Bagheri, K. Al-jabery, D. Wunsch and J. Burken, A deeper look at plant uptake of environmental contaminants using intelligent approaches, *Sci. Total Environ.*, 2018, **651**, 561–569, DOI: **10.1016/j.scitotenv.2018.09.048**.

34 Y. Si, H. Huang, J. Pan, X. Luo, J. Zhang, Y. Guo, *et al.*, Identification of potential biomarkers and pathways involved in high-altitude pulmonary edema using GC-MS and LC-MS metabolomic methods, *Sci. Rep.*, 2024, **14**(1), 30978, DOI: **10.1038/s41598-024-82047-w**.

35 S. Martínez, Evaluación de marcadores físico-químicos y metabolómicos con mayor incidencia en la maduración heterogénea de la plata (*Persea americana*) variedad Hass, Universidad Nacional Agraria La Molina, *Food industry engineering*, thesis, 2020, available from: **https://repositorio.lamolina.edu.pe/items/c187f754-2ce6-43e6-b860-cc6ada47f0c1**.

36 E. Padilla-Camberos, M. Martínez-Velázquez, J. M. Flores-Fernández and S. Villanueva-Rodríguez, Acute toxicity and genotoxic activity of avocado seed extract (*Persea americana* Mill., c.v. Hass), *Sci. World J.*, 2013, 1–4, DOI: **10.1155/2013/245828**.

37 I. Hernández, V. Uarrota, C. Fuentealba, D. Paredes, B. G. Defilippi and R. Campos-Vargas, Transcriptome and hormone analyses reveals differences in physiological age of 'Hass' avocado fruit, *Postharvest Biol. Technol.*, 2022, **185**(2), 111806, DOI: **10.1016/j.postharvbio.2021.111806**.

38 C. Camacho-Vázquez, J. M. Elizalde-Contreras, F. A. Reyes-Soria, J. L. Monribot-Villanueva, J. A. Guerrero-Analco, J. Juarez-Escobar, *et al.*, Towards Characterization of Hass Avocado Peel and Pulp Proteome during Postharvest Shelf Life, *Proteomes*, 2024, **12**(28), 1–16, DOI: **10.3390/proteomes12040028**.

39 C. T. Lara-García, H. Jiménez-Islas and R. Miranda-López, Perfil de compuestos orgánicos volátiles y ácidos grasos del aguacate (*Persea americana*) y sus beneficios a la salud, *CienciaUAT*, 2021, **16**(1), 162–177, DOI: **10.29059/cienciauat.v16i1.1483**.

40 D. G. Rodríguez-Sánchez, A. Pacheco, R. Villarreal-Lara, M. R. Ramos-González, P. A. Ramos-Parra, S. Granados-Principal, *et al.*, Chemical Profile and Safety Assessment of a Food-Grade Acetogenin-Enriched Antimicrobial Extract from Avocado Seed, *Molecules*, 2019, **24**(13), 2354, DOI: **10.3390/molecules24132354**.

41 J. A. Villa-Rodriguez, E. M. Yahia, A. González-León, I. Ifie, R. E. Robles-Zepeda and J. A. Domínguez-Avila, Ripening of 'Hass' avocado mesocarp alters its phytochemical profile and the *in vitro* cytotoxic activity of its methanolic extracts, *S. Afr. J. Bot.*, 2020, **128**, 1–8, DOI: **10.1016/j.sajb.2019.09.020**.

42 V. G. Uarrota, I. Hernández, E. Ponce, C. M. Bauer, M. Maraschin and R. Pedreschi, Metabolic profiling and biochemical analysis of stored Hass avocado fruit by GC-MS and UHPLC-UV-VIS revealed oxidative stress as the main driver of 'blackspot' physiological disorder, *Int. J. Food Sci. Technol.*, 2022, **57**(12), 7896–7916, DOI: **10.1111/ijfs.16145**.

43 D. J. Bhuyan, M. A. Alsherbiny, S. Perera, M. Low, A. Basu, O. A. Devi, *et al.*, The Odyssey of Bioactive Compounds in Avocado (*Persea americana*) and Their Health Benefits, *Antioxidants*, 2019, **8**(10), 426, DOI: **10.3390/antiox8100426**.

44 K. Matsui, Green leaf volatiles: hydroperoxide lyase pathway of oxylipin metabolism, *Curr. Opin. Plant Biol.*, 2006, **9**(3), 274–280, DOI: **10.1016/j.pbi.2006.03.002**.

45 E. Castro-Mercado, Y. Martinez-Diaz, N. Roman-Tehandon and E. Garcia-Pineda, Biochemical analysis of reactive oxygen species production and antioxidative responses in unripe avocado (*Persea americana* Mill. var Hass) fruits in response to wounding, *Protoplasma*, 2009, **235**(1–4), 67–76, DOI: **10.1007/s00709-009-0034-y**.

46 A. Leone, T. Bleve-Zacheo, C. Gerardi, M. Melillo, L. Leo and G. Zacheo, Lipoxygenase Involvement in Ripening Strawberry, *J. Agric. Food Chem.*, 2006, **54**(18), 6835–6844, DOI: **10.1021/jf061457g**.

47 J. Hu, A. Baker, B. Bartel, N. Linka, R. T. Mullen, S. Reumann, *et al.*, Plant peroxisomes: biogenesis and function, *Plant Cell*, 2012, **24**(6), 2279–2303, DOI: **10.1105/tpc.112.096586**.

48 B. Halliwell and J. M. C. Gutteridge, *Free Radicals in Biology and Medicine*, Oxford University Press, 2015, available from: DOI: **10.1093/acprof:oso/9780198717478.001.0001**.

49 N. Dudareva, F. Negre, D. Nagegowda and I. Orlova, Plant Volatiles: Recent Advances and Future Perspectives, *CRC Crit. Rev. Plant Sci.*, 2006, **25**(5), 417–440, DOI: **10.1080/07352680600899973**.

50 I. Feussner and C. Wasternack, The lipoxygenase pathway, *Annu. Rev. Plant Biol.*, 2002, **53**, 275–297, DOI: **10.1146/annurev.arplant.53.100301.135248**.

51 D. W. Crabb, M. Matsumoto, D. Chang and M. You, Overview of the role of alcohol dehydrogenase and aldehyde dehydrogenase and their variants in the genesis of alcohol-related pathology, *Proc. Nutr. Soc.*, 2004, **63**(1), 49–63, DOI: **10.1079/pns2003327**.

52 J. Fürstenberg-Hägg, M. Zagrobelny and S. Bak, Plant Defense against Insect Herbivores, *Int. J. Mol. Sci.*, 2013, **14**(5), 10242–10297, DOI: **10.3390/ijms140510242**.

53 A. Ayala, M. F. Muñoz and S. Argüelles, Lipid peroxidation: production, metabolism, and signaling mechanisms of malondialdehyde and 4-hydroxy-2-nonenal, *Oxid. Med. Cell. Longevity*, 2014, **2014**(1), 360438, DOI: **10.1155/2014/360438**.

54 R. L. Shewfelt and B. A. Rosario, The Role of Lipid Peroxidation in Storage Disorders of Fresh Fruits and Vegetables, *HortScience*, 2000, **35**(4), 575–579, DOI: **10.21273/HORTSCI.35.4.575**.

55 M. Murali and T. Shivanandappa, Endosulfan causes oxidative stress in the liver and brain that involves inhibition of NADH dehydrogenase and altered antioxidant enzyme status in rat, *Ecotoxicol. Environ. Saf.*, 2022, **239**(1), 113593, DOI: **10.1016/j.ecoenv.2022.113593**.

56 A. Hatanaka, T. Kajiwara and K. Matsui, The Biogeneration of Green Odour by Green Leaves and It's Physiological Functions – Past, Present and Future, *Zeitschrift für Naturforschung C*, 1995, **50**, 467–472, DOI: **10.1515/znc-1995-7-801**.

57 S. Bak, F. Beisson, G. Bishop, B. Hamberger, R. Höfer, S. Paquette, *et al.*, Cytochromes p450, *Arabidopsis Book*, 2011, **9**, e0144, DOI: **10.1199/tab.0144**.

58 R. Končitíková, A. Vigouroux, M. Kopečná, T. Andree, J. Bartoš, M. Šebela, *et al.*, Role and structural characterization of plant aldehyde dehydrogenases from family 2 and family 7, *Biochem. J.*, 2015, **468**(1), 109–123, DOI: **10.1042/BJ20150009**.

59 E. Skrzypczak-Jankun, R. A. Bross, R. T. Carroll, W. R. Dunham and M. O. Funk, Three-Dimensional Structure of a Purple Lipoxygenase, *J. Am. Chem. Soc.*, 2001, **123**(44), 10814–10820, DOI: **10.1021/ja011759t**.

60 E. K. Bomati and J. P. Noel, Structural and Kinetic Basis for Substrate Selectivity in Populus tremuloides Sinapyl Alcohol Dehydrogenase, *Plant Cell*, 2005, **17**(5), 1598–1611, DOI: **10.1105/tpc.104.029983**.

61 C. E. Christensen, B. B. Kragelund, P. von Wettstein-Knowles and A. Henriksen, Structure of the human β-ketoacyl [ACP] synthase from the mitochondrial type II fatty acid synthase, *Protein Sci.*, 2007, **16**(2), 261–272, DOI: **10.1110/ps.062473707**.

62 J. G. Olsen, A. V. Rasmussen, P. von Wettstein-Knowles and A. Henriksen, Structure of the mitochondrial β-ketoacyl-[acyl carrier protein] synthase from *Arabidopsis* and its role in fatty acid synthesis, *FEBS Lett*, 2004, **577**(1–2), 170–174, DOI: **10.1016/j.febslet.2004.10.007**.

63 H. Inoue and J. M. Lowenstein, Acetyl coenzyme A carboxylase from rat liver. EC 6.4.1.2 acetyl-CoA: carbon dioxide ligase (ADP), *Methods Enzymol.*, 1975, **35**, 3–11, DOI: **10.1016/0076-6879(75)35131-8**.

64 H. Zhang, Z. Yang, Y. Shen and L. Tong, Crystal Structure of the Carboxyltransferase Domain of Acetyl-Coenzyme A Carboxylase, *Science*, 2003, **299**(5615), 2064–2067, DOI: **10.1126/science.1081366**.

65 L. Pedersen and A. Henriksen, Acyl-CoA Oxidase 1 from *Arabidopsis thaliana*. Structure of a Key Enzyme in Plant Lipid Metabolism, *J. Mol. Biol.*, 2005, **345**(3), 487–500, DOI: **10.1016/j.jmb.2004.10.062**.

66 M. J. Maté, M. Zamocky, L. M. Nykyri, C. Herzog, P. M. Alzari and C. Betzel, Structure of catalase-A from *Saccharomyces cerevisiae*, *J. Mol. Biol.*, 1999, **286**(1), 135–149, DOI: **10.1006/jmbi.1998.2453**.

67 J. P. Betancourt-Arango, A. Patiño-Ospina, J. A. Fiscal-Ladino and G. Taborda-Ocampo, Volatilomic Analysis in Peel, Pulp and Seed of Hass Avocado (*Persea americana* Mill.) From the Northern Subregion of Caldas by Gas Chromatography With Mass Spectrometry, *Food Sci. Nutr.*, 2025, **13**(7), e70489, DOI: **10.1002/fsn3.70489**.

68 M. Alonso-Trujillo, A. B. Muñiz-González and J. L. Martínez-Guitarte, Endosulfan exposure alters transcription of genes involved in the detoxification and stress responses in *Physella acuta*, *Sci. Rep.*, 2020, **10**(1), 7847, DOI: **10.1038/s41598-020-64554-8**.